ANALYSIS OF HAT-SECTIONED REINFORCED COMPOSITE BEAMS INCLUDING THERMAL EFFECTS

by

KASHIF ALI NAYYER SYED

Presented to the Faculty of the Graduate School of

The University of Texas at Arlington in Partial Fulfillment

of the Requirements

for the Degree of

DOCTOR OF PHILOSOPHY

THE UNIVERSITY OF TEXAS AT ARLINGTON

December 2006

To my lovely grand parents, Abba, Ammi, Phuppu-jaan and Maqbool mam

ACKNOWLEDGEMENTS

I would like to express my sincere appreciation and gratitude to my supervising professor, Dr. Wen S. Chan, Mechanical and Aerospace Engineering Department, for his guidance, patience and encouragement. My pursuit of a doctoral degree was profoundly based upon his character and integrity. I would like to express my sincere thanks to Dr. John H. Matthys, Dr. Guillermo Rameriz, Dr. Nur Yazdani and Dr. Anand Puppala, committee members, for their valuable advice and assistance.

A special and sincere acknowledgement to the former chairman of the Department of Civil Engineering at the University of Texas at Arlington, Dr. Siamak Ardekani, for his understanding, guidance and financial support throughout my academic program. Special thanks and grateful acknowledgement is due to Dr. Puppala for been a constant source of support.

Finally, I would like to thank my mother, father and sisters, Didi and Sara, for their never-ending support and love, and special acknowledgement is due to my relatives, Dr. Azher unsari Saab, Mazher bhaiya, Nayeem mama, Shammas, Sajid bhai and Arshad bhai for their moral support, understanding and encouragement, which made this dissertation possible.

November 20, 2006

ABSTRACT

ANALYSIS OF HAT-SECTIONED REINFORCED COMPOSITE BEAMS INCLUDING THERMAL EFFECTS

Publication No. _____

Kashif Ali Nayyer Syed, Ph.D.

The University of Texas at Arlington, 2006

Supervising Professor: Wen S. Chan

A simple analytical method for analyzing fiber reinforced polymeric composite beams with hat cross-section is presented. The method includes development of closed-form expression of the axial, bending and their coupling stiffness matrices for the composite beams. The stiffness matrices are obtained by transforming the actual geometrical cross-section of the beam into an equivalent plate using transformation matrices and Parallel Axis theorem. Ply stresses due to mechanical as well as thermal load can easily be obtained at any given location of the beam section. In this approach, the effect of induced in-plane deformation due to bending for an unsymmetrical cross-section is included while the conventional analysis, using the smeared properties, ignores this coupling effect. Finite element analysis was conducted to obtain the results for comparison. It is concluded that the axial and bending stiffness obtained by the present method gives excellent agreement to the finite element results as compared

with the conventional method. Significant error is observed for axial stiffness comparison between conventional and finite element results. Experimental bending stiffness values of I-beams are also used for comparison and good conformity is observed using present method.

A simple closed form solution is derived based on the extensional application of developed method to obtain ply stresses due to thermal loading. Results were validated and excellent agreement is observed with the finite element model.

Location of centroid and shear center plays an important role in engineering analysis as extension/bending and bending/twisting are decoupled at these locations, respectively. For composite material, these locations are dependent not only on cross sectional geometry but also on the material properties. Based on the stiffness matrices obtained, a simple methodology is developed to determine these locations. Results are validated by comparing with isotropic materials and also by observing the behavior of composite material for symmetric and unsymmetric cases. It is concluded that the present method provides generic solution for the design and analysis of laminated composite beams with significant accuracy and ease. The developed tool is handy in providing the parametric study for composite structural design.

TABLE OF CONTENTS

LIST OF ILLUSTRATIONS

LIST OF TABLES

CHAPTER 1

INTRODUCTION

1.1 Background

The civil engineering industry is constantly striving for ways to improve design and construction technologies to obtain a more economical solution to engineering problems. Fiber Reinforced Polymer (FRP) Composites are very attractive for use in civil engineering applications due to their unique benefits. FRP composites have been widely used in the aerospace, military and the automotive industries for many years. They are used routinely and extensively in structural components of both military and commercial aircraft. Recently, civil and off-shore structures just began using composite material as an alternative to the conventional materials. Their basic advantages are free-form and tailored design characteristics, high strength-weight and stiffness-weight ratios, good corrosion and fatigue resistance, ease of manufacturing and construction, and low maintenance cost, compared to steel and concrete, the traditional construction materials. However, FRP composites usually exhibit complicated mechanical behavior due to the anisotropic material properties.

During the 1990s and into the new millennium the utilization of advanced polymer composite materials have made large advances in civil engineering construction field, specifically bridges. A couple of all-composite bridge decks are

already in use, such as, Laurel Lick Bridge in Lewis County, WV and Wickwire Run Bridge in Taylor County, WV [1].

Despite their availability and diversity, civil engineers are hesitant to design with FRP composites because the design of composite structures is quite complicated and need specialized training, also due to the absence of design criteria and guidelines. Engineers have to use expensive tools, such as the finite element method, in order to analyze and optimize their designs. The use of sophisticated analyses can be time consuming, and therefore, simple but yet sufficiently accurate analytical tools are needed to be able to predict the response of FRP structural components and systems.

1.2 Literature Review on Composite Beams

In structural applications, beam with thin-walled cross-section is one of the most efficient structural members that can achieve the required stiffness with minimum weight. In structural analysis, most structures are often analyzed as beams as one-dimensional structural members if one dimension (the length) is much larger than the other two dimensions (width and thickness). The foundation of the beam analysis is based upon the moment-curvature relationship along the longitudinal axis of the beam. This approach used for laminated composite beam is not different from the isotropic beam. However, in evaluation of the moment-curvature relationship, so-called the bending stiffness of the beam, laminated composite beam possesses a unique behavior that is different from the isotropic beam.

The analysis of composite beam has been extensively studied for sometimes. Several textbooks that included composite beam analysis were published [2-6]. Analytical methods presented in those books are too complicated to be used in design practice. In composite beam analysis of civil structural applications, McGhee et al. [7] performed a numerical analysis on fiber reinforced plastics decks of different shapes based on the experimental studies carried out by Henry [8] and Ahmad and Plecnik [9]. Zurieck [10] has conducted a finite-element analysis on simply supported FRP decks. Among those studies, smeared property of composite section was used in their analysis. In analysis of composite tubular beams, Chan and his co-workers [11, 12] include ply orientation change due to the beam section contour in formulating their stiffness model. Their results indicated that using smear property for computing bending stiffness of composite tubular section can results in significant error in bending stiffness.

Stresses are induced in composite laminates when subjected to temperature change. Hussein, Fazio, and Ha [14] studied the effects of bonding stiffness in sandwich panels subjected to uniform temperature change and gradient temperature change. Sandwich panels were made of thin skins and a lightweight core, which have different coefficient of thermal expansion. Experimental results were in good agreement with theory. It was found that thermal stresses are a function of material properties of sandwich skin and core, and also the rigidity between skin and core. A sandwich panel with a flexible core may not produce significant thermal stresses. If the core had some rigidity then temperature change will induce thermal stresses. Also difference in

coefficient of thermal expansion of skin and core play an important role in thermal stresses [15]

Finite element method is often used in the analysis of composite structures. Although the computer capability has been tremendously increased in the past decades, analysis by using FEM is still not an efficient method because of structural configuration dependent. Hence, finite element analysis is not an effective method to perform a parametric study, particularly in the preliminary design stage in which final configuration of composite structure is not well determined yet.

Therefore, designing composite beams has a need for analytical methods that not only provide accurate evaluation of sectional property for better prediction of structural response but also can be easily used for parametric study.

1.3 Objective of the Research

The fundamental objective of the research is to develop a closed form solution for composite beams, using lamination theory and translation of axis theorem by simplifying the three-dimensional beam into a two dimensional plate. The focus of this study is on understanding the behavior of hat-sectioned reinforced composite beam due to various loading. Results are compared and validated by performing finite element analysis of fully three-dimensional constructed models in ANSYS software.

In the present approach, the effect of induced in-plane deformation due to bending for an unsymmetrical cross-section is included while the conventional analysis ignores this coupling effect. Equations are derived for inclined composite laminate and simple methodology of dividing entire cross-section into individual laminates and then

mapping them to a common axis is used. Once the stiffness matrices of the entire cross-section are obtained, important properties of beam like axial stiffness, bending stiffness, centroid and shear center can easy be extracted. In addition, ply stress of each layer can be obtained for given loading case. Thermal loading is also applied and ply stresses are obtained. In isotropic material, thermal strains are produced due to applied thermal loading and thermal stresses are produced only when there is a constraint. However, composite materials exhibit complicated behavior under thermal loading, thermal stress is a function of stacking sequence and it is produced in addition of thermal strains even without global constraint.

AS4/3501-6 Graphite/Epoxy is selected for analysis. In finite element analysis, axial and bending stiffness are obtained by applying the corresponding axial and bending loads. Ply stresses are obtained for the applied bending load and thermal loading.

1.4 Outline of the Dissertation

Chapter 2 gives a detail description of the analytical method developed and equations derived using lamination theory.

Chapter 3 contains the description of analytical method developed for thermal analysis.

Chapter 4 deals with the methodology developed to evaluate centroid and shear center of the hat cross-section.

Chapter 5 lists the conclusions and recommendations.

CHAPTER 2

ANALYTICAL STIFFNESS MATRIX SOLUTION OF COMPOSITE HAT-SECTION

This chapter is devoted to the development of an analytical solution for composite beams with hat cross-section using lamination theory and parallel axis theorem. Conventionally, in the analysis of composite beam, the smeared mechanical properties of the composite beam cross-section were often used. In doing so, the effect of induced in-plane deformation due to bending for an unsymmetrical cross-section is ignored. The present analysis takes this effect into account in development of structural stiffness.

2.1 Geometry of Composite Hat Cross-Section

Hat cross-section is divided into individual laminates. As shown in Figure 2.1, let b_{tf} be the width of top flange, b_{bf} is the width of bottom flanges, b_b is the width of bottom laminate, t_{ply} is the thickness of each ply, b_w is the width of web and H is the vertical height. It should be noted that b_{tf}, b_{bf} and H are kept constant, where as b_w and b_{bl} varies according to web angle, $\sin^{-1}(H/b_w)$. Hence, b_b is dependent of the angle.

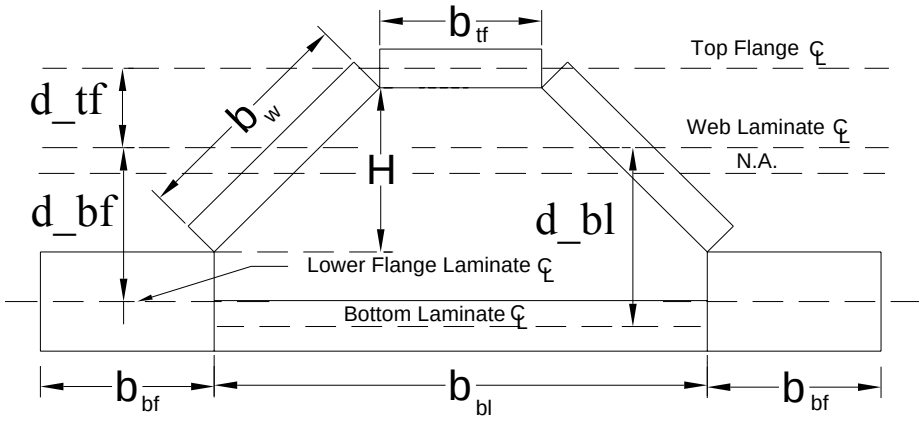

Figure 2.1 Geometry of Hat Cross-Section

2.2 Stress-Strain Relationship for Orthotropic Lamina

For a thin layer of composite lamina, it can be assumed that the lamina is under plane stress condition in the direction of lamina thickness [16]. Under plane stress condition, all the stress components in the out-of-plane direction are zero. That is,

$$\sigma_3 = \tau_{13} = \tau_{23} = 0$$

Therefore, the stress-strain relationship in principal material coordinates can be expressed in matrix as follows:

$$\begin{bmatrix} \sigma_1 \\ \sigma_2 \\ \tau_{12} \end{bmatrix} = \begin{bmatrix} Q_{11} & Q_{12} & 0 \\ Q_{21} & Q_{22} & 0 \\ 0 & 0 & Q_{66} \end{bmatrix} \cdot \begin{bmatrix} \varepsilon_1 \\ \varepsilon_2 \\ \gamma_{12} \end{bmatrix} = [Q_{1-2}] \cdot \begin{bmatrix} \varepsilon_1 \\ \varepsilon_2 \\ \gamma_{12} \end{bmatrix} \tag{2.1}$$

Where $[Q_{1-2}]$ is called as reduced stiffness matrix and the subscripts 1,2 and 6 refer to the properties along the fiber, transverse to the fiber and shear in the plane, respectively.

The matrix $[Q_{1-2}]$ in terms of engineering constants is given as:

$$Q_{11} = \frac{E_1}{1-\nu_{12}\nu_{21}}$$

$$Q_{22} = \frac{E_2}{1-\nu_{12}\nu_{21}} \tag{2.2}$$

$$Q_{12} = \frac{\nu_{12}E_2}{1-\nu_{12}\nu_{21}}$$

$$Q_{66} = G_{12}$$

Where E_1 and E_2 are the Young's moduli of lamina along and transverse to the fiber direction, respectively. ν_{12} is the Poisson's ratio and G_{12} is the shear modulus of lamina under a loading along the fiber direction.

2.3 Classical Lamination theory

Laminated composite is composed of multiple thin orthotropic plies of anisotropic material. Classical Lamination Theory (CLT) is most commonly used to analyze the behavior of laminated composite and also to evaluate strains and stresses of plies in the laminate. To analyze the behavior of laminate, CLT treats laminate as an equivalent single layered plate. The structural response of laminate is represented by the strains and curvatures about its mid-plane. Strains and stresses at any point in the k^{th} ply can be calculated using the following relationship:

$$\begin{bmatrix} \varepsilon_x \\ \varepsilon_y \\ \gamma_{xy} \end{bmatrix} = \begin{bmatrix} \varepsilon_x^0 \\ \varepsilon_y^0 \\ \gamma_{xy}^0 \end{bmatrix} + z \begin{bmatrix} k_x \\ k_y \\ k_{xy} \end{bmatrix} \tag{2.3}$$

Where ε_x^0, ε_y^0 and γ_{xy}^0 are the mid-plane strains, κ_x, κ_y and κ_{xy} are the mid-plane curvatures, z is the coordinate measured from the mid-plane to the lamina and ε_x, ε_y and γ_s are the strains in the k^{th} ply.

$$\begin{bmatrix}\sigma_x\\ \sigma_y\\ \tau_s\end{bmatrix}=\begin{bmatrix}\overline{Q}_{xx} & \overline{Q}_{xy} & \overline{Q}_{xs}\\ \overline{Q}_{yx} & \overline{Q}_{yy} & \overline{Q}_{ys}\\ \overline{Q}_{sx} & \overline{Q}_{sy} & \overline{Q}_{ss}\end{bmatrix}\cdot\begin{bmatrix}\varepsilon_x^0\\ \varepsilon_y^0\\ \gamma_s^0\end{bmatrix}+z\begin{bmatrix}\overline{Q}_{xx} & \overline{Q}_{xy} & \overline{Q}_{xs}\\ \overline{Q}_{yx} & \overline{Q}_{yy} & \overline{Q}_{ys}\\ \overline{Q}_{sx} & \overline{Q}_{sy} & \overline{Q}_{ss}\end{bmatrix}\cdot\begin{bmatrix}k_x\\ k_y\\ k_s\end{bmatrix} \tag{2.4}$$

Where $[\overline{Q}_{x-y}]_k$ is a symmetric matrix and is obtained by transforming [$Q_{1\text{-}2}$] matrix of lamina from 1-2 material coordinates to the laminate x-y coordinates. The details on obtaining $[\overline{Q}_{x-y}]_k$ are shown in Appendix A.

2.3.1 Laminate Constitutive Equation

The in-plane forces [N] and moments [M] (per unit length) are obtained by integrating forces of each ply through the laminate thickness, that is, integrating equation 2.4 as shown below:

$$N_x=\int_{-h}^{h}\sigma_x dz \qquad N_y=\int_{-h}^{h}\sigma_y dz \qquad N_{xy}=\int_{-h}^{h}\tau_{xy} dz$$

$$M_x=\int_{-h}^{h}z\sigma_x dz \qquad M_y=\int_{-h}^{h}z\sigma_y dz \qquad M_{xy}=\int_{-h}^{h}z\tau_{xy} dz \tag{2.5}$$

Where ‘h’ is the distance from the reference plane to the plate’s surfaces. Ply stresses are related in terms of mid-plane strains and curvatures; hence, general load-deformation relation of laminate is obtained in terms of mid-plane strain and curvature as shown below:

$$\begin{bmatrix}N\\ M\end{bmatrix}=\begin{bmatrix}A & B\\ B & D\end{bmatrix}\cdot\begin{bmatrix}\varepsilon^0\\ \kappa\end{bmatrix} \tag{2.6}$$

Where,

$$[N]=\sum_{k=1}^{n}\int_{Z_{K-1}}^{Z_K}[\sigma]_k\cdot dz \tag{2.7}$$

$$[M] = \sum_{k=1}^{n} \int_{Z_{K-1}}^{Z_K} [\sigma]_k \cdot z \cdot dz \tag{2.8}$$

$$[A] = \sum_{k=1}^{n} [\overline{Q}_{x-y}]_k (z_k - z_{k-1}) \tag{2.9}$$

$$[B] = \frac{1}{2} \sum_{k=1}^{n} [\overline{Q}_{x-y}]_k (z_k^2 - z_{k-1}^2) \tag{2.10}$$

$$[D] = \frac{1}{3} \sum_{k=1}^{n} [\overline{Q}_{x-y}]_k (z_k^3 - z_{k-1}^3) \tag{2.11}$$

Where z_k and z_{k-1} represent the z-coordinate of the top and bottom surface of the k^{th} layer, respectively. $[\overline{Q}_{x-y}]_k$ is the stiffness matrix of k^{th} layer, which is function of the material constant and its ply orientation. [A], [B], and [D] are the sub-matrices of global stiffness matrix. They refer to the in-plane stiffness (also called as extensional stiffness), the coupling stiffness, and the bending stiffness for the laminate, respectively.

2.3.2 Parallel Axis Theorem applied for Laminate Axis Transformation

Using lamination theory, stiffness matrices are usually obtained about the mid-plane of a laminate. If a structural component is an assembly of laminates, oriented on different locations, it becomes necessary to translate stiffness matrices to a common reference axis in order to obtain stiffness matrix of entire structure. Parallel axis theorem is used for this purpose. If "d" is the distance measured from the old reference axis to the new reference axis as shown in figure, we have

$$z_k^{'} = z_k + d \tag{2.12}$$

Therefore, the modified stiffness matrices, $[A]', [B]' and [D]'$, which are referred to the new axis, can be obtained as,

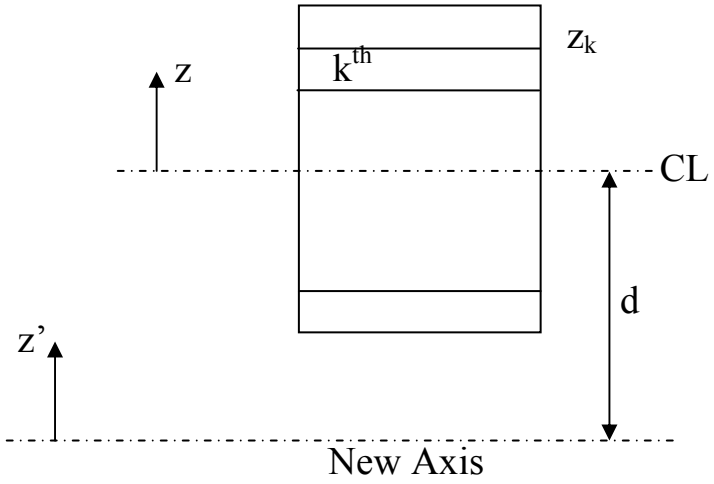

Figure 2.2 Axis Translation

$$[A]' = [A]$$

$$[B]' = [B] + d \cdot [A] \tag{2.13}$$

$$[D]' = [D] + 2d \cdot [B] + d^2 \cdot [A]$$

2.4 Stiffness Model of Composite Hat-Section

In this section, equations are derived for inclined laminate by considering the reference axis about the mid-height and about the base of the web. Then the stiffness matrices for the top and bottom laminates as well as web laminates are translated to the reference axis of the hat-section.

2.4.1 Axial and Bending Stiffness of the Flange and Bottom Laminates

The *[A], [B],* and *[D]* matrices for the top and bottom flange laminates with respect to its own mid-plane of each laminate can be easily obtained by the composite lamination theory (CLT). These matrices calculated by CLT are based upon the unit width of laminates. Hence, the total stiffness matrices of the flange laminates can be obtained by multiplying the width of each laminate.

2.4.2 Stiffness of Web Laminates about Mid-height

The mid-height axis of the web laminate is selected as the reference axis for the stiffness derivation. The web laminate is inclined at an angle θ with respect to reference axis. Consider an infinitesimal element of the web laminate along the width direction, as shown in Figure 2.3. Let "ds" be the width of infinitesimal element of the laminate at a distance S from the reference axis. The element is first rotated about x'-axis (onto y'-z' coordinate system) and then translated to the selected reference axis of the cross-section. After this process, the axial and bending stiffness can be obtained by integration of the stiffness of the element along the entire length of the web laminate.

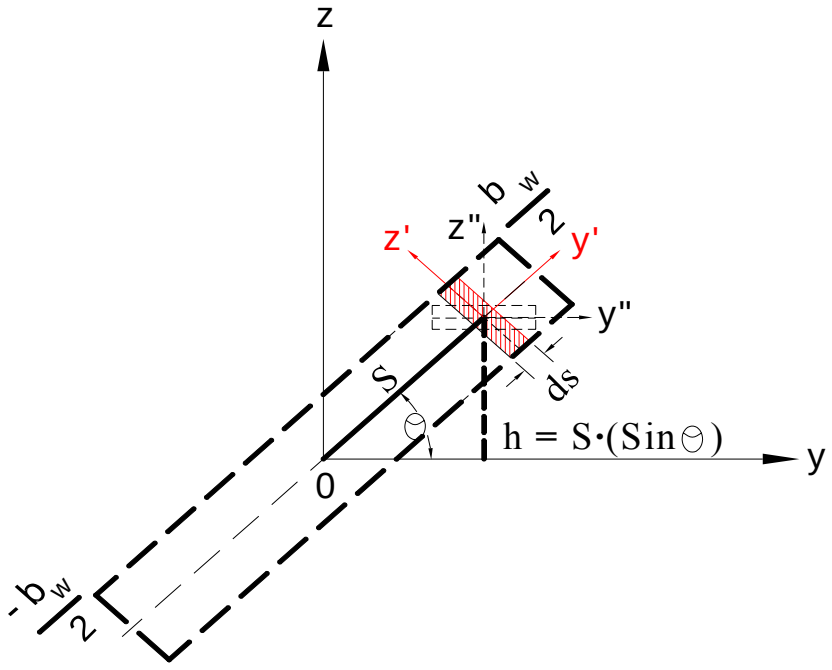

Figure 2.3 Infinitesimal Section of Web laminate (about Mid-height)

Using parallel axis theorem, transformed stiffness matrices for the element are given as,

$$[A] = [A'']$$

$$[B] = [B''] + h \cdot [A'']$$

$$[D] = [D''] + 2 \cdot h \cdot [B''] + h^2 \cdot [A'']$$

Where, $h = S \cdot Sin\theta$

Integrating along the length of the laminate, we have,

$$\left[\overline{A}\right]_W = \int_{-b_w/2}^{b_w/2} [A'']_W \cdot ds = b_w \cdot [A'']_W$$

$$\left[\overline{B}\right]_W = b_w \cdot [B'']_W + \int_{-b_w/2}^{b_w/2} (S \cdot Sin\theta) \cdot ds \cdot [A'']_W = b_w \cdot [B'']_W$$

$$\left[\overline{D}\right]_W = b_w \cdot [D'']_W + 2 \cdot \int_{-b_w/2}^{b_w/2} (S \cdot Sin\theta) \cdot ds \cdot [B'']_W + \int_{-b_w/2}^{b_w/2} (S \cdot Sin\theta)^2 \cdot ds \cdot [A'']_W$$

$$= b_w \cdot [D'']_W + \frac{b_w^3}{12} \cdot Sin^2\theta \cdot [A'']_W$$

Hence,

$$\left[\overline{A}\right]_w = b_w \cdot [A'']_w$$

$$\left[\overline{B}\right]_w = b_w \cdot [B'']_w \qquad (2.14)$$

$$\left[\overline{D}\right]_w = b_w \cdot [D'']_w + \frac{b_w^3}{12} \cdot Sin^2\theta \cdot [A'']_w$$

$[A'']_w$, $[B'']_w$ and $[D'']_w$ are the stiffness per unit width and are given as

$$[A'']_w = \sum_{k=1}^{n} \left[\overline{Q}''_{x-y}\right]_k \cdot (z''_k - z''_{k-1})$$

$$[B'']_w = \frac{1}{2}\sum_{k=1}^{n}\left[\overline{Q}''_{x-y}\right]_k \cdot \left(z''^2_k - z''^2_{k-1}\right) \tag{2.15}$$

$$[D'']_w = \frac{1}{3}\sum_{k=1}^{n}\left[\overline{Q}''_{x-y}\right]_k \cdot \left(z''^3_k - z''^3_{k-1}\right)$$

2.4.3 Reduced ply stiffness of web laminate

Let 1-2-3 (or z') be the material principal coordinates, x'-y'-z' be the inclined web laminate coordinates (see Fig. 2.3), x"-y"-z" be the web laminate coordinates parallel to the x-y-z coordinates, the coordinates of the global cross section. The 3- and x'- axes are coincided to the z'- and x-axes, respectively. $[Q_{1\text{-}2}]$ is the reduced stiffness matrix of a composite ply. The subscripts, 1and 2 refer to the properties along the fiber and transverse to the fiber direction, respectively. The 3- or z'- axis is normal to 1-2 plane.

The angle ply stiffness can be obtained by first rotating the infinitesimal element θ (the web angle) about x'-axis. The infinitesimal element is then rotated with its fiber orientation β angle around the z'- axis. The overall ply stiffness in the x-y-z coordinates can be written as:

$$\left[\overline{Q}''_{x-y}\right]_k = \left[T_\sigma(-\beta)\right]_z \cdot \left[T_\sigma(-\theta)\right]_x \cdot \left[Q_{1-2}\right] \cdot \left[T_\varepsilon(+\theta)\right]_x \cdot \left[T_\varepsilon(+\beta)\right]_z \tag{2.16}$$

$[T_\sigma]$ and $[T_\varepsilon]$ in the above equation are the stress and strain transformation matrices, respectively. The subscripts, x and z in $[T_\sigma]$ and $[T_\varepsilon]$ indicate the axes where the stiffness matrix is rotated. The expression of $[T_\sigma]$ and $[T_\varepsilon]$ matrices are given in Appendix. The explicit form of the stiffness matrix in equation 2.16 for the ply in the web is given in Appendix (A.17).

2.4.4 Stiffness of Web Laminates about Base

In certain cross-sections like hexagonal cross section it may be convenient to use the base of the laminate as the reference axis to find the stiffness matrices. Consider laminate of length 'L' inclined at an angle θ with respect to local x axis. Let 'ds' be the width of infinitesimal element of the laminate at a distance 'S' from the base of laminate as shown in figure below. The vertical distance of the element is represented as 'h'.

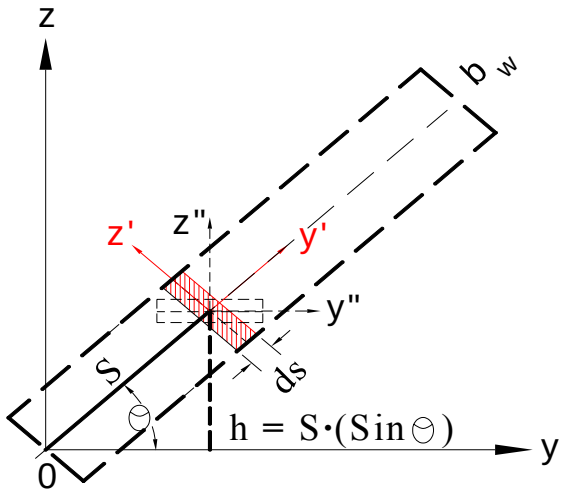

Figure 2.4 Infinitesimal Section of Web laminate (about Base)

Integrating along the length of the laminate, we have,

$$\left[\overline{A}\right]_W = \int_0^{b_w} \left[A''\right]_W \cdot ds = b_w \cdot \left[A''\right]_W$$

$$\left[\overline{B}\right]_W = b_w \cdot \left[B''\right]_W + \int_0^{b_w} (S \cdot Sin\theta) \cdot ds \cdot [A'']_W = b_w \cdot [B'']_W + \frac{b_w^2}{2} \cdot Sin\theta \cdot [A'']_W$$

$$\left[\overline{D}\right]_W = b_w \cdot \left[D''\right]_W + 2 \cdot \int_0^{b_w} (S \cdot Sin\theta) \cdot ds \cdot [B'']_W + \int_0^{b_w} (S \cdot Sin\theta)^2 \cdot ds \cdot [A'']_W$$

$$= b_w \cdot [D'']_W + b_w^2 \cdot Sin\theta \cdot [B'']_W + \frac{b_w^3}{3} \cdot Sin^2\theta \cdot [A'']_W$$

Hence,

$$\left[\overline{A}\right]_W = b_w \cdot \left[A''\right]_W$$

$$\left[\overline{B}\right]_W = b_w \cdot \left[B''\right]_W + \frac{b_w^2}{2} \cdot Sin\theta \cdot [A'']_W \qquad (2.17)$$

$$\left[\overline{D}\right]_W = b_w \cdot \left[D''\right]_W + b_w^2 \cdot Sin\theta \cdot [B'']_W + \frac{b_w^3}{3} \cdot Sin^2\theta \cdot [A'']_W$$

2.4.5 Overall Constitutive Equation of Hat Cross-section

The overall stiffness matrices of the hat-section are the sum of the stiffness matrices of each laminates. The stiffness matrices of each laminates have to be translated to the common reference axis before the summation. The bending stiffness of a beam section depends on the location of the bending axis. In obtaining this stiffness of isotropic material beam with any given cross section, it is customarily to select the neutral axis as a reference axis where no axial stress/strain exists. For the case of isotropic material, the location of the neutral axis is only dependent on geometry of the cross-section. However, for laminated composite beam, the location of this axis depends not only on the geometry of the cross section but also on the ply orientation, the stacking sequence and material properties of each segment of the laminate. Hence, for the composite beam with a hat cross-section, the reference axis can be arbitrarily selected. In doing so, the axial stress/strain at this location may not be zero. In the derivation of the following stiffness matrices, the reference axis for the hat cross-section is initially selected as the mid-height of the web. The overall section stiffness is then evaluated at neutral axis.

2.4.6 Axial and Bending Stiffness of Narrow Beam

The structural response of the beam is dependent on ratio of the width to the height of the cross-section [17]. If the width to height ratio of the beam cross section is very large, the induced transverse curvature along the edge due to bending is insignificant. This kind of the beam is termed as a wide flange beam. For this case, a non-zero moment, M_y is induced to constraining the induced curvature in the transverse direction. Conversely, if the width to height ratio is small, the beam is then termed as a narrow flange beam. For this case, κ_y can not be constrained. As a result, no moment, M_y is induced. For all of the cases studied, the width to height ratio ranges from 3 to 6, approximately, which is considered as a small value. Hence, the present beam will be considered as a narrow beam. The constitutive equation shown above was based upon the laminated plate theory. Equation 2.6 can be rewritten as:

$$\begin{bmatrix} \bar{\varepsilon}^o \\ \bar{\kappa} \end{bmatrix} = \begin{bmatrix} \bar{a} & \bar{b} \\ \bar{b}^T & \bar{d} \end{bmatrix} \cdot \begin{bmatrix} N \\ M \end{bmatrix} \tag{2.18}$$

Where,

$$\begin{bmatrix} \bar{a} & \bar{b} \\ \bar{b}^T & \bar{d} \end{bmatrix} = \begin{bmatrix} \bar{A} & \bar{B} \\ \bar{B} & \bar{D} \end{bmatrix}^{-1} \tag{2.19}$$

For a narrow beam, Equation 2.18 is written as

$$\begin{bmatrix} \varepsilon_x^o \\ \kappa_x \end{bmatrix} = \begin{Bmatrix} a_{11} & b_{11} \\ b_{11} & d_{11} \end{Bmatrix} \begin{bmatrix} N_x \\ M_x \end{bmatrix} \tag{2.20}$$

The axial and bending stiffness of the beam are then given as:

$$(EA)_{beam} = \frac{d_{11}}{a_{11} \cdot d_{11} - b_{11}^2} \tag{2.21}$$

$$(EI)_{beam} = \frac{a_{11}}{a_{11} \cdot d_{11} - b_{11}^2} \tag{2.22}$$

Above equations enforces zero curvature and zero axial strain when evaluating *EA* and *EI*, respectively. Hence, $(EI)_{beam}$ in equation 2.22 will be considered as the bending stiffness at the neutral axis. This equation was also used to calculate the axial and bending stiffness of a laminated beam with a delamination [18].

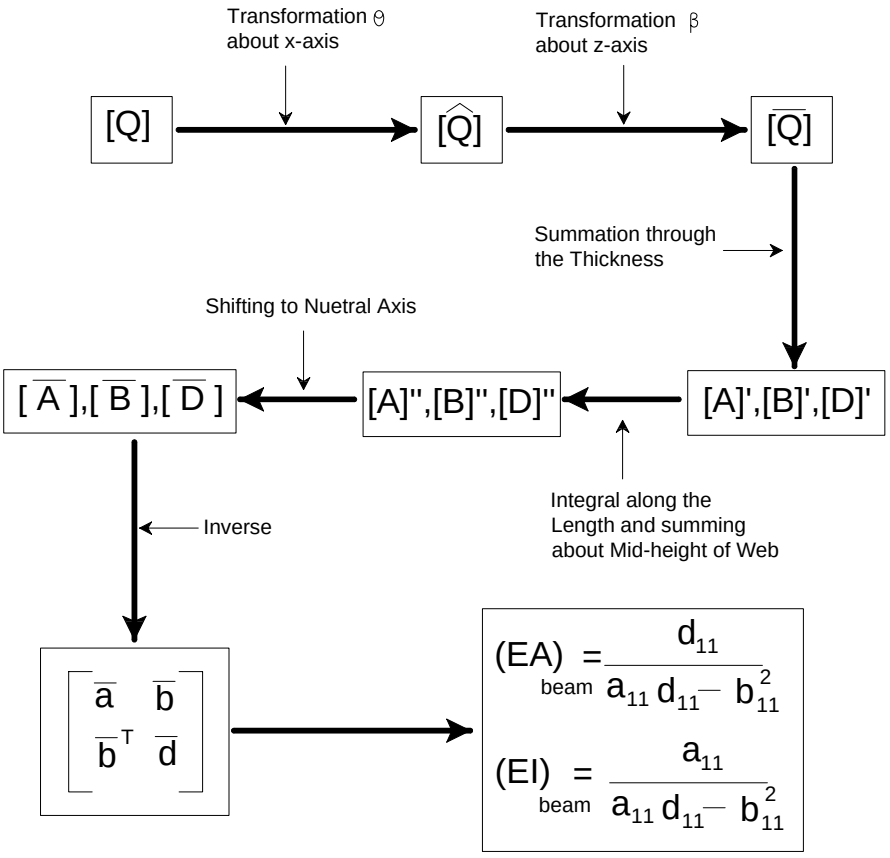

Figure 2.5 Flow chart to calculate Axial and Bending Stiffness

2.5 Ply Stress Calculation

Stress in any k^{th} ply at a distance z_k from mid-plane is computed using the Stress-Mid plane strain-curvature relationship shown in equation 2.4. The mid-plane strains and curvatures are acquired using equation 2.19. General form of equation 2.4 to compute stress in any ply is given below:

$$[\sigma_k]_{x-y} = [\overline{Q}]_k \cdot [\overline{\varepsilon}]_k \quad = [\overline{Q}]_k \cdot ([\overline{\varepsilon}_0] + z_k \cdot [\overline{\kappa}_0]) \tag{2.23}$$

Where, $[\overline{Q}]_k$ is the transformed ordinary reduced stiffness matrix of the k^{th} layer corresponding to the vertical distance z_k from mid-plane.

2.6 Finite Element Analysis

Finite element model (FEM) was developed to obtain the results which were used to compare the results obtained by the present closed form solution. Since interests of this study were on the stiffness and in-plane ply stresses of the beam, a two-dimensional finite element model was employed.

2.6.1 Model Description

The model is generated in ANSYS [19]. Input file is used to create the model and Graphical User Interface (GUI) is used for post processing. The mesh of the model is built using bottom-up construction procedure, that is, key points are defined first and then areas are formed by connecting those key points, lines are automatically generated from areas. The model contains 12 key points, 18 lines, 6 areas, 4046 nodes and 1320 elements. The length of the model is 20 inches long.

Two-dimensional shell element, SHELL91 was selected. The element has eight nodes and each node has six degrees of freedom: three translations and three rotations in

x, y, and z directions. The property of the element is defined by layer thicknesses, layer material direction angles, and orthotropic material properties. The lay-up sequence of each segment of the hat section is shown in result section. However, it should be noted that the bottom layer of the cross-section is unsymmetrical; figure 2.5 shows the lay-up sequence of the bottom anti-symmetric laminate. The entire cross-section is not symmetric with respect to the reference axis of the cross-section. Hence, the coupling effects between bending and in-plane load exist.

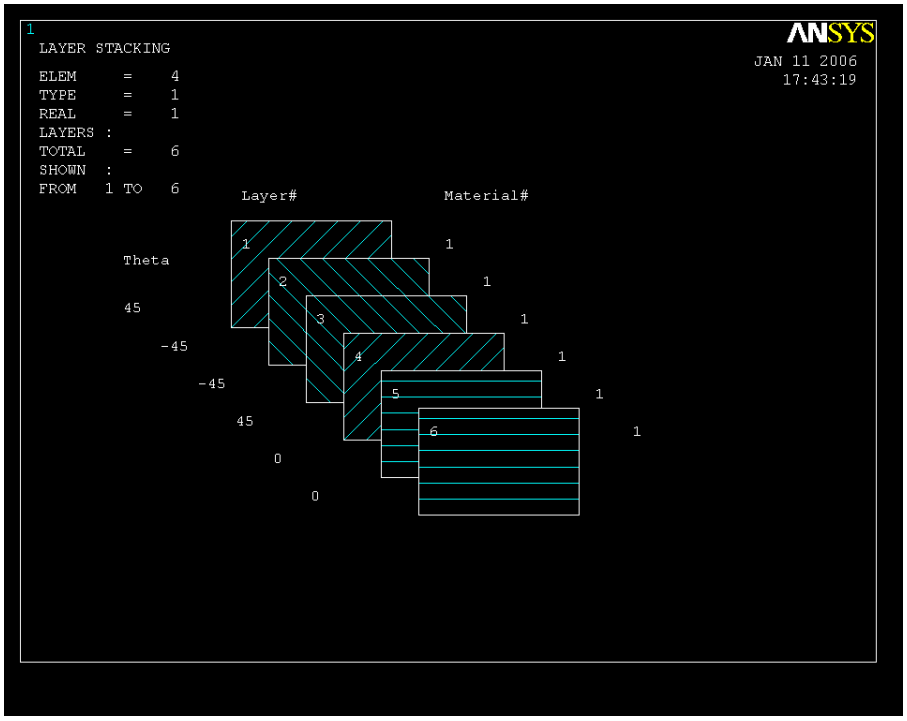

Figure 2.6 Layer stacking sequence of bottom anti-symmetric laminate

For the axial load case, the model is fixed at one end and an axial load is applied at the other end. Command CP is used to ensure uniform displacement across the hat section along the loading direction. Figure 2.7 gives a graphical representation of applied end conditions to evaluated axial stiffness.

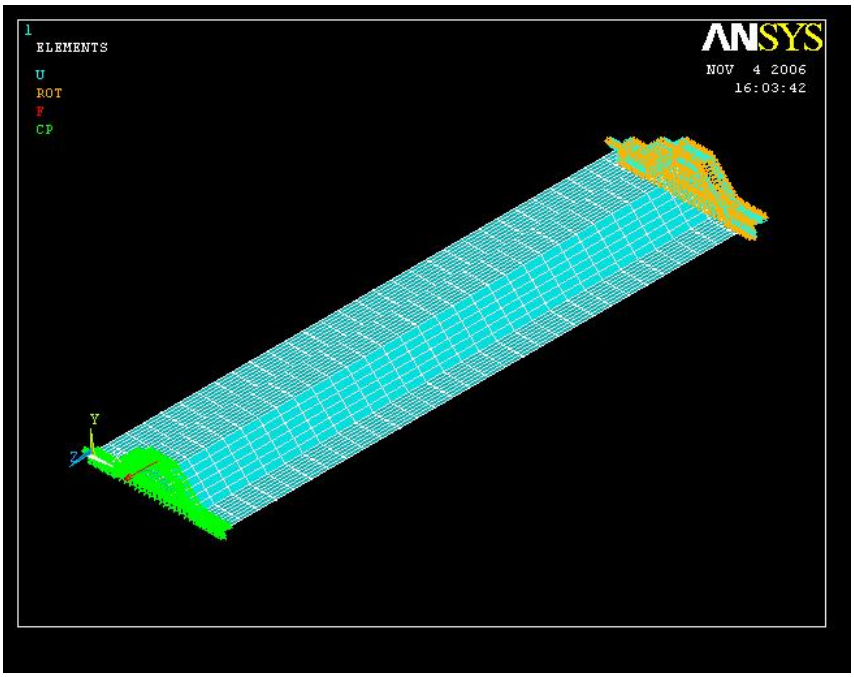

Figure 2.7 Applied End Conditions for Axial Load Case

For the bending case, the model is fixed at one end and the moment is applied by a couple of forces in the opposite direction at the other end. Command CERIG is used to create rigid region connecting given set of nodes to one node called 'master node'. This connection ensures relative constraints in displacements and rotations. Figure 2.6 gives a pictorial representation of the loading end conditions.

Convergence study was conducted in order to obtain optimum mesh size. Meshing that generates elements ranging from 300 to 2000 at an approximate increment of 300 where used. Insignificant variation in the bending stiffness value was observed, however, the convergence was observed to be near 1320 elements. This mesh is used in the study for all the beams.

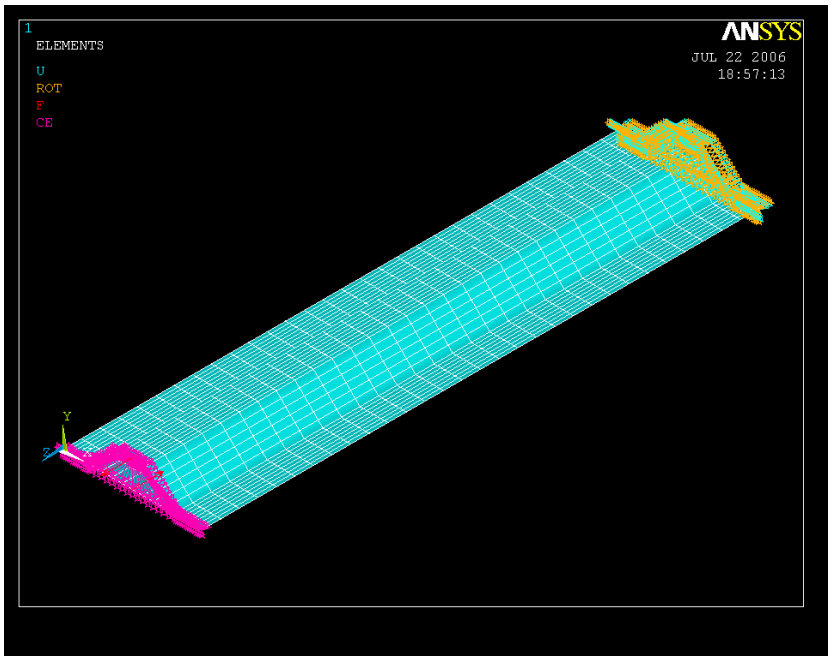

Figure 2.8 Applied End Conditions for Bending Case

2.6.2 Stiffness Calculation from FEM model

The bending stiffness for any given hat section beam is obtained by relating the curvature of the deformed beam to the applied moment. The curvature of the deformed beam is calculated by recording the displacements in x and z directions of any three points on the same plane. From these displacements, the curvature of the deformed beam can be obtained [20]. Hence,

$$(EI)_{beam} = \rho \cdot M_{applied} \tag{2.24}$$

Where, ρ is the radius of curvature and M is the applied moment.

The axial stiffness is simply obtained by dividing the applied axial load by strain along that direction as given by,

$$(EA)_{beam} = {P_{applied}}/{\varepsilon_x} \tag{2.25}$$

2.6.3 Verification of the FEM model

To validate the FEM model and the present approach, aluminum material was first used to implement to all of the models. Data and dimension of the model are shown in table 2.1

TABLE 2.1

MATERIAL PROPERTIES AND DIMENSIONS OF THE ISOTROPIC MODEL

Name	**Values**
Elastic Modulus, E (psi)	10E+06
Poisson's Ratio, ν	0.33
Widths, b_{tf} and b_{bf} (in)	1
Thickness, t_{tf}, t_{bf}, t_w and t_{bl} (in)	0.03, 0.05, 0.02 and 0.03 respectively
Web Height, H (in)	1
Coupling Force	100 lb

The comparison of axial and bending stiffness between strength of mechanics approach and finite element results are tabulated in tables 2.2 and 2.3, respectively. The value obtained from FEM model of the laminated hat-section beam shows good agreement with one calculated using solid mechanics. This clearly proves the validity of the finite element model using isotropic material. Hence, this model can be applied to orthotropic material.

TABLE 2.2

COMPARISON OF AXIAL STIFFNESS OF HAT SECTION MADE OF ISOTROPIC MATERIAL

AXIAL STIFFNESS, EA, kips			
Web Angle, θ	Strength of Mechanics Approach	FEM Solution	**Difference**
90	2000	2035	**+1.7 %**
75	2175	2215	**+1.8 %**
60	2410	2454	**+1.8 %**
45	2762	2821	**+2.1 %**
30	3440	3515	**+2.1 %**

TABLE 2.3

COMPARISON OF BENDING STIFFNESS OF HAT SECTION MADE OF ISOTROPIC MATERIAL

BENDING STIFFNESS, EI, 10^3 lb-in^2			
Web Angle, θ	Strength of Mechanics Approach	FEM Solution	**Difference**
90	324.4	312.6	**-3.8 %**
75	337.3	322.2	**-4.7 %**
60	356.3	339.3	**-5.0 %**
45	388.0	368.4	**-5.3 %**
30	452.1	427.3	**-5.8 %**

2.7 Numerical Examples and Results

The geometry and lay-up sequence used for composite hat section are shown in section 2.7.1. The results are presented in section 2.7.2 and 2.7.3.

2.7.1 Geometry and Lay-up Sequence of Composite Section

Results of analytical solution are obtained by the code written in MATLAB. On the other hand, finite element results are obtained by ANSYS. The beams with various web angles, θ, were studied but the height of the cross-section remains constant. The width of the bottom laminate varies with respect to θ. The geometry of hat-section studied is shown in figure 2.9. The material used in this study was AS4/3501 graphite epoxy laminates. Its properties are listed in table 2.4

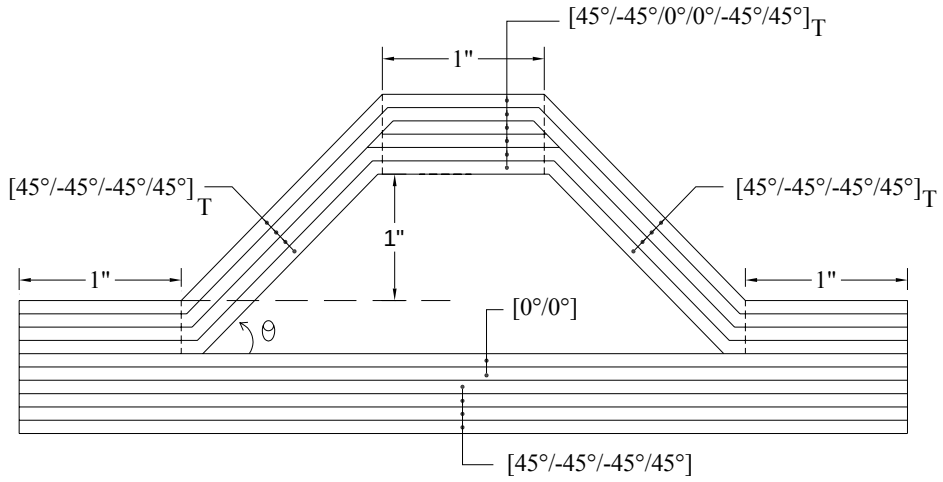

Figure 2.9 Geometry and Lay-up sequence of Composite Hat-Section

2.7.2 Deflection and Deformation of Composite Beams

Figure 2.10 shows the contour plot of the deformed shape of the beam subjected to an axial load. As indicated, the beam exhibit a uniform axial deformation with a very

small curvature induced due to its unsymmetry across the thickness of the cross-section. Figure 2.11 shows the deflected shape of the cross-section due to bending. A negligible twisting deformation is observed.

TABLE 2.4

MATERIAL PROPERTIES FOR AS4/3501-6
GRAPHITE/EPOXY LAMINATE

AS4/3501-6 Graphite/Epoxy	
Properties	Value
E_{11}	18.2E6 psi
E_{22}	1.41E6 psi
G_{12}	0.92E6 psi
ν_{12}	0.274
t_{ply}	0.005”

2.7.3 Stiffness Comparison between Conventional, Present and FEM Model of Composite Section

Bending and axial stiffness of composite hat-section with various web angles are investigated. The web angle is varied at 15 degrees ranging from 30˚ to 90˚ as tabulated below. Table 2.5 and Table 2.6 list the axial stiffness and bending stiffness of the cross section, respectively. As indicated, the results obtained by the present method are in an excellent agreement with the FEM results for both axial and bending cases. Moreover, the results obtained from the conventional method are far from the FEM results for the case of axial load. Since each laminate segment of the cross section in the FEM model is well connected. In the present and conventional methods, no constraint between

segments is involved. Hence, the FEM results are in a higher bound. For the bending case, the great amount of bending stiffness for the entire cross-section is contributed by the top and bottom flanges. Hence, the difference between the FEM results compared to the conventional and present methods are relative small with respect to the web angle change. Furthermore, the conventional method ignored the coupling effect between axial and bending of the entire cross-section.

TABLE 2.5

COMPARISON OF EFFECTIVE AXIAL STIFFNESS BETWEEN CONVENTIONAL, PRESENT AND FEM RESULTS

AXIAL STIFFNESS, EA, 10^3 lb					
Web Angle, θ	**Conventional Method [a]**	**Present Method [b]**	**FEM Result [c]**	**Difference between [c]& [a]**	**Difference between [c]& [b]**
90	937.0	1182.7	1230.0	+23.8 %	**+3.8 %**
75	1020.0	1317.4	1370.0	+25.6%	**+3.8 %**
60	1126.0	1478.5	1540.0	+26.9 %	**+4.0 %**
45	1283.0	1705.2	1780.0	+27.9 %	**+4.2 %**
30	1571.0	2107.3	2220.0	+29.2 %	**+5.1 %**

The time required to run ANSYS input file and extract axial and bending stiffness value, for a given beam case, is approximately 23 minutes. Where as, the time required to run MATLAB code and extract axial and bending stiffness value, for a given beam case, is just 2 seconds.

TABLE 2.6

COMPARISON OF EFFECTIVE BENDING STIFFNESS BETWEEN CONVENTIONAL, PRESENT AND FEM RESULTS

BENDING STIFFNESS, EI, 10^3 lb-in^2					
Web Angle, θ	**Conventional Method [a]**	**Present Method [b]**	**FEM Result [c]**	**Difference between [c] & [a]**	**Difference between [c] & [b]**
90	196.0	210.8	210.8	7.0 %	**0.0 %**
75	205.3	219.0	219.0	6.3 %	**0.0 %**
60	215.9	230.4	230.4	6.3 %	**0.0 %**
45	230.7	247.8	247.8	6.9 %	**0.0 %**
30	257.0	278.9	278.9	7.9 %	**0.0 %**

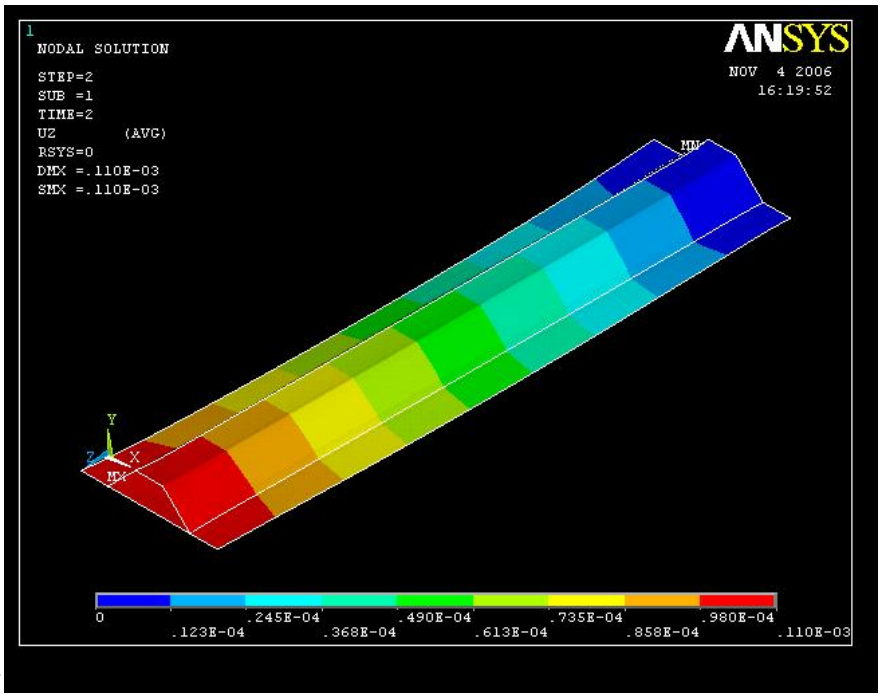

Figure 2.10 Contour Plot of Deformed Shape due to Axial Load

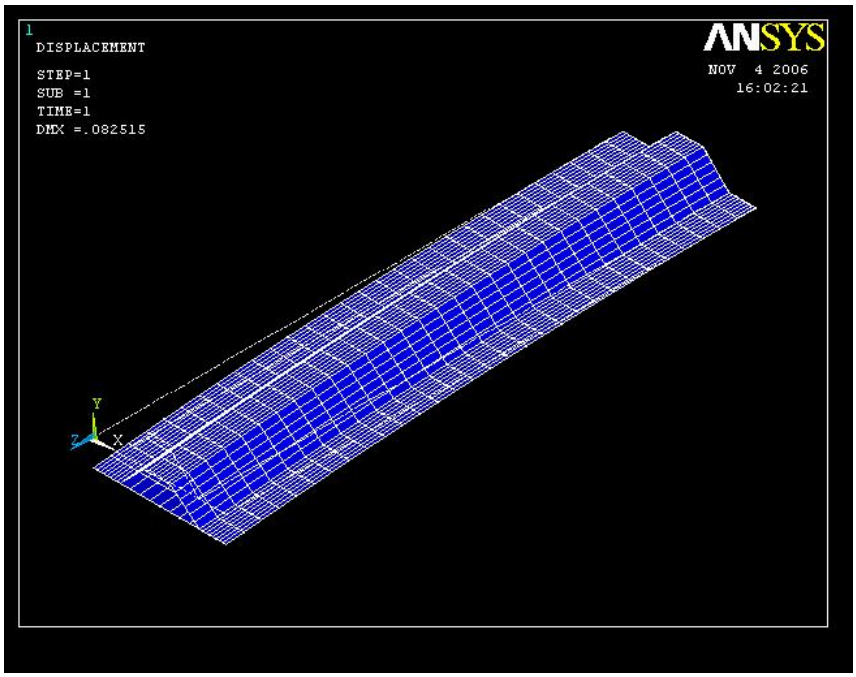

Figure 2.11 Deflected Shape due to Applied Moment at Free End

2.7.4 Ply Stress Comparison

The stresses in any ply of the hat beam with a web angle of 45˚ were investigated. A coupling force of 100 lb is applied at the free end resulting in pure bending across the length of the beam. Consequently, ply stresses at any cross-section along the length of the beam remains constant.

Figures 2.12 and 2.13 shows the ANSYS result of σ_x distribution of hat-section. A uniform stress distribution along the beam axis (longitudinal axis) is observed. A comparison of σ_x distribution calculated by the FEM and the present method is shown in figures 2.14 and 2.15. The excellent agreement is observed in the figure. The location of the neutral axis where $\sigma_x=0$ is in agreement between two different approach.

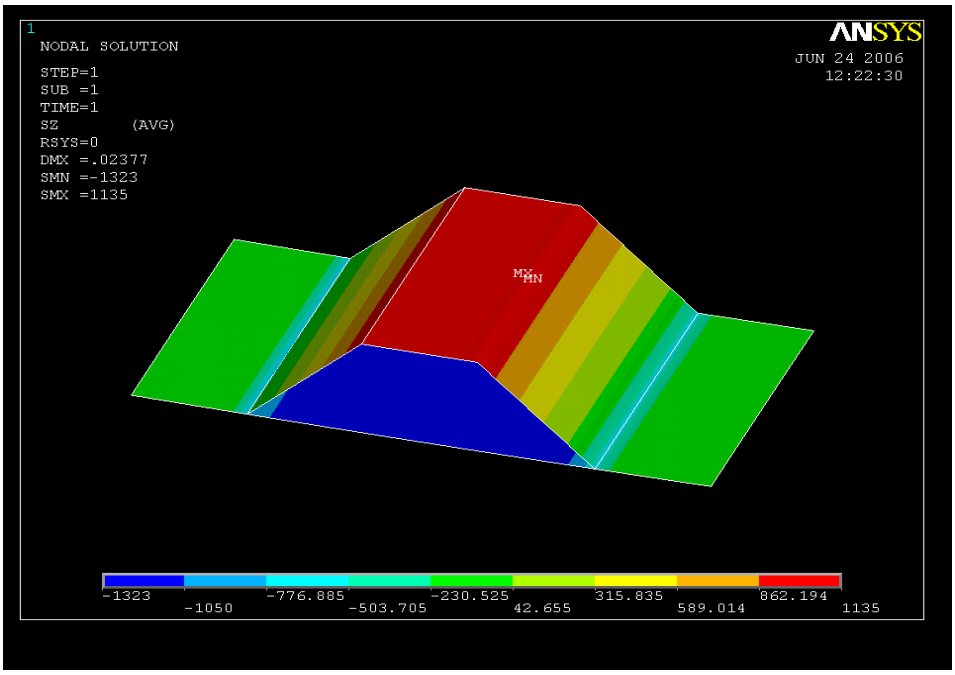

Figure 2.12 Contour Plot of σ_x in Top Plies with 45° Web Angle

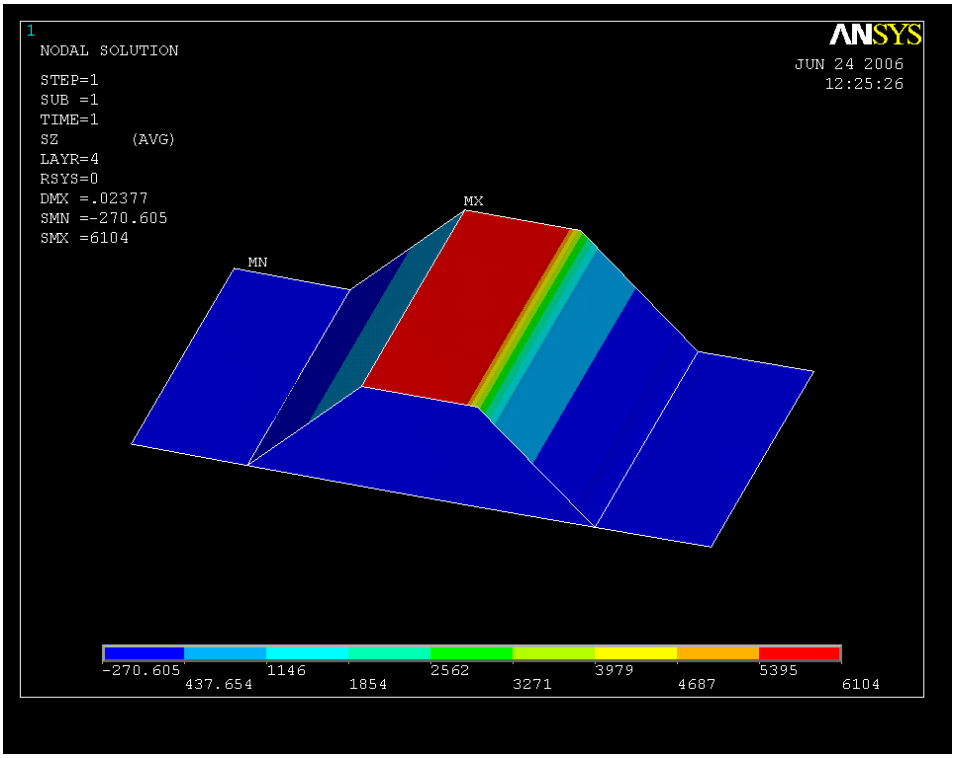

Figure 2.13 Contour Plot of σ_x in Top 0° Ply with 45° Web Angle

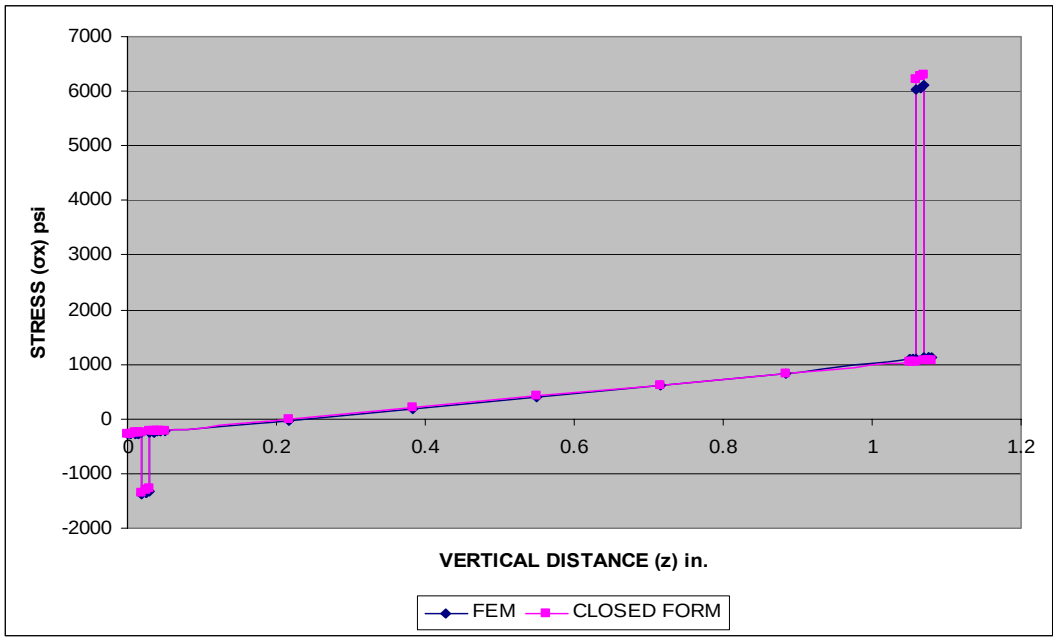

Figure 2.14 Comparison of σ_x in all plies of hat-section with 45° web angle

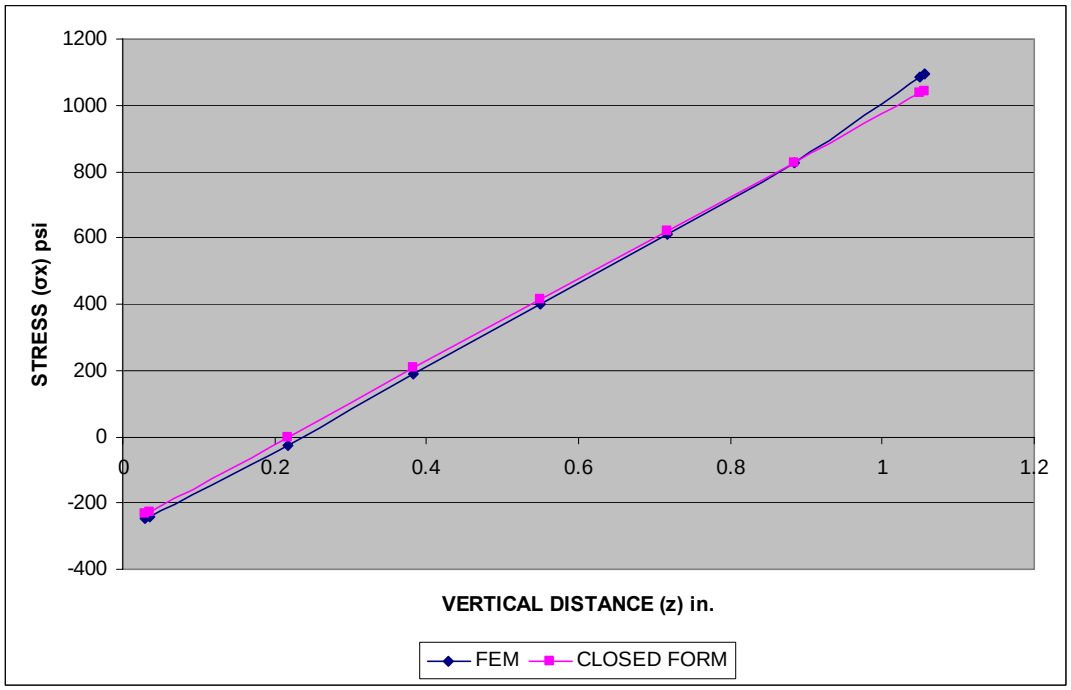

Figure 2.15 Comparison of σ_x in 45° ply of Hat-Section with 45° web angle

2.8 Experimental Bending Stiffness of I-Beam

Bending stiffness of I-beam obtained experimentally by [20] is compared using the present approach. Excellent agreement is observed between the present approach and experimental values as tabulated below:

TABLE 2.7

COMPARISON OF EFFECTIVE BENDING STIFFNESS VALUES OF EXPERIMENTAL I-BEAM

BENDING STIFFNESS, EI, 10^3 lb-in^2				
Top Flange Width (in.)	**Bottom Flange Width (in.)**	**EI_{exp}**	$\overline{D}_{11}^{*}$	**Present Method**
2.460	2.458	587	697 (15.7 %)	**596 (-1.5%)**
2.195	2.203	530	611 (13.3 %)	**520 (1.9%)**
1.936	1.924	480	568 (15.5 %)	**477 (0.6%)**
1.471	1.480	424	462 (8.2 %)	**413 (2.6%)**
1.257	1.263	364	397 (8.2 %)	**355 (2.5%)**
1.141	1.330	350	393 (8.2 %)	**352 (-0.6%)**
0.774	0.788	256	288 (11.0 %)	**248 (3.1%)**

2.9 Delamination

Delamination is defined as the fracture of the plane separating two plies of laminated composite structure. This fracture occurs within the thin resin-rich layer that forms between plies during the manufacturing process or when subjected to load. It is a major concern in the structural performance of composite materials. Delamination often results in a loss of stiffness and strength, and may lead to safety and reliability problems, making this one of the major obstacles in achieving the full weight saving potential of advanced composite materials.

Delaminations occur at stress free edges due to the mismatch in properties of the individual layers, at ply drops where thickness must be reduced, at regions subjected to out-of-plane loading such as bending of curved beams. Delaminations form due to some combination of three basic fracture modes. These include the opening mode (Mode I), the sliding shear mode (Mode II), and the scissoring shear mode (Mode III). Usually, to predict the onset and growth of delamination, the interlaminar fracture toughness (IFT) associated with each of the fracture modes is characterized and the corresponding strain energy release rates for each mode associated with the configuration and loading of interest is calculated. Chan and Chou [18] developed an analytical method using sub-laminate approach to quantify the loss of stiffness due to presence of delamination in laminate. Lin and Chan [12] applied the same approach to elliptical cross-section and validated using Finite Element Analysis to study the loss of stiffness due to delamination.

The most common sources of delamination are the material and structural discontinuities. Figure 2.16 shows the common sources of delamination at geometric and material discontinuities.

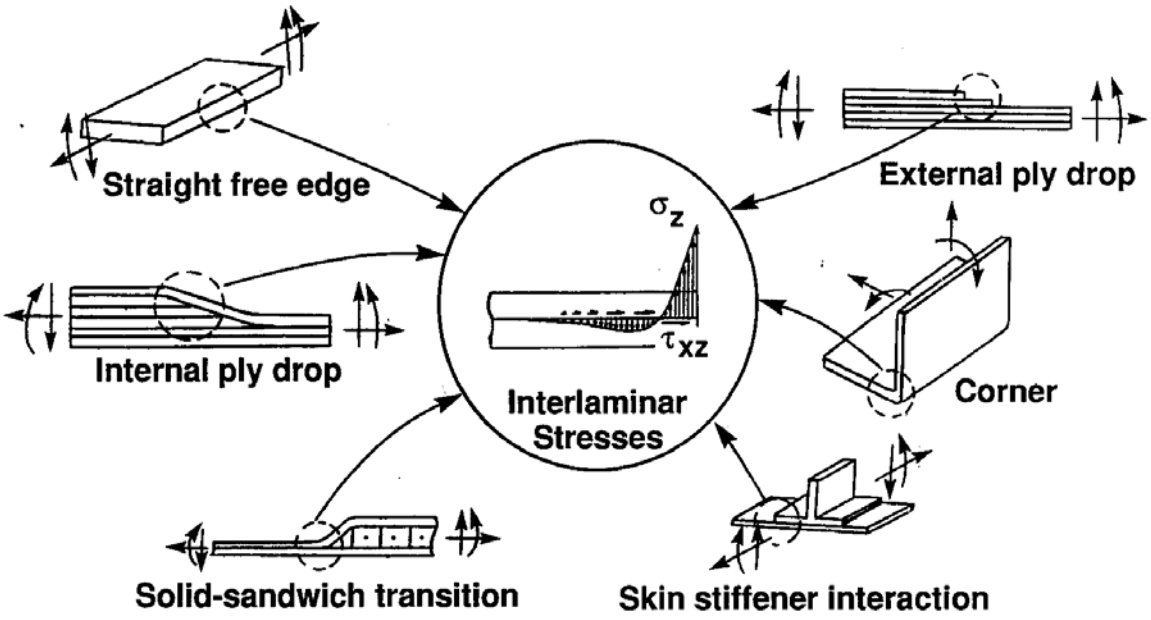

Figure 2.16 Delamination Sources at Geometric and Material Discontinuities

For the Hat-Cross Section studies, the expected type of delamination is due to the "Skin stiffener interaction" as shown in the figure, which is the debonding of the foot of the stiffener from the plate.

CHAPTER 3

ANALYTICAL SOLUTION FOR THERMAL ANALYSIS

Fiber-reinforced composite materials are generally processed at an elevated temperature and then cooled down to room temperature. If an unconstrained composite laminate is subjected to a uniform change in temperature, in-plane stresses will be induced due to the constraint configuration of each lamina of the cross section and also due to the coefficients of thermal expansion. Consequently, most modern composite laminates where laminas are placed at different angles are subjected to a significant state of stress prior to the application of any external mechanical loading.

In chapter 2, an analytical solution for calculating ABD matrix for hat-section was developed. The ABD matrix is not altered by inclusion of thermal loading since the ABD matrix is only dependent of laminate elastic properties and geometry. However, the stress-strain relationship and residual stresses in plies will be altered.

3.1 Free Thermal Response of Composite Hat-section

The geometry, lay-up sequence and material properties of hat-section studied here are the same as the one studied in chapter 2. A uniform temperature, ΔT, of 100˚F is applied and ply stresses will be induced. It should be noted that for graphite/epoxy lamina coefficient of thermal expansion (CTE), which relates strains to temperature change, along the fiber direction (α_1) is -0.5e-6 in/in/˚F and transverse to the fiber direction (α_2) is 15e-6 in/in/˚F. Therefore, increase in temperature will cause decrease

in fiber direction. However, stress produced along the fiber direction will be negligible because of the negligible CTE value. For 0˚ ply, the dominate thermal stress will be along y-direction (σ_y) and for angle ply, say 45˚, the dominate thermal stress is the shear stress caused due the shear stains and the secondary stress will be along the y-direction.

3.1.1 Unit Thermal Force and Moment Resultants

By integrating stresses through the thickness of the laminate, force and moment resultants can be defined as [13]:

$$N_x^T = \Delta T \cdot \sum_{k=1}^{n} \left(\overline{Q}_{11}^k \overline{\alpha}_x^k + \overline{Q}_{12}^k \overline{\alpha}_y^k + \overline{Q}_{16}^k \overline{\alpha}_{xy}^k \right) \cdot \left(h_k - h_{k-1} \right)$$

$$N_y^T = \Delta T \cdot \sum_{k=1}^{n} \left(\overline{Q}_{12}^k \overline{\alpha}_x^k + \overline{Q}_{22}^k \overline{\alpha}_y^k + \overline{Q}_{26}^k \overline{\alpha}_{xy}^k \right) \cdot \left(h_k - h_{k-1} \right)$$

$$N_{xy}^T = \Delta T \cdot \sum_{k=1}^{n} \left(\overline{Q}_{16}^k \overline{\alpha}_x^k + \overline{Q}_{26}^k \overline{\alpha}_y^k + \overline{Q}_{66}^k \overline{\alpha}_{xy}^k \right) \cdot \left(h_k - h_{k-1} \right) \tag{3.1}$$

$$M_x^T = \frac{\Delta T}{2} \cdot \sum_{k=1}^{n} \left(\overline{Q}_{11}^k \overline{\alpha}_x^k + \overline{Q}_{12}^k \overline{\alpha}_y^k + \overline{Q}_{16}^k \overline{\alpha}_{xy}^k \right) \cdot \left(h_k^2 - h_{k-1}^2 \right)$$

$$M_y^T = \frac{\Delta T}{2} \cdot \sum_{k=1}^{n} \left(\overline{Q}_{12}^k \overline{\alpha}_x^k + \overline{Q}_{22}^k \overline{\alpha}_y^k + \overline{Q}_{26}^k \overline{\alpha}_{xy}^k \right) \cdot \left(h_k^2 - h_{k-1}^2 \right)$$

$$M_{xy}^T = \frac{\Delta T}{2} \cdot \sum_{k=1}^{n} \left(\overline{Q}_{16}^k \overline{\alpha}_x^k + \overline{Q}_{26}^k \overline{\alpha}_y^k + \overline{Q}_{66}^k \overline{\alpha}_{xy}^k \right) \cdot \left(h_k^2 - h_{k-1}^2 \right)$$

These quantities are material properties, just as the ABD is, and they yield the thermal stress and moment resultants by simply multiplying them by the temperature change, ΔT. $\left[\overline{Q}\right]_k$ is the transformed reduced stiffness matrix for z-axis rotation only and $\left[\overline{\alpha}\right]$ is the transformed coefficient of thermal expansion matrix.

3.1.2 Parallel Axis theorem applied to transfer Force and Moment resultants

Force and Moment resultant obtained using equation 3.1 act along the mid-plane of the laminate. Parallel axis theorem is used to transfer these resultants to a reference axis, which is the mid-plane of the web laminate for the entire hat-section. If "d" is the distance measured from the old reference axis to the new reference axis as shown in figure 2.2 of chapter 2,

We have,

$$\overline{h}_k = h_k + d\,;\ \overline{h}_{k-1} = h_{k-1} + d \tag{3.2}$$

$$\overline{N}_x^T = \Delta T \cdot \sum_{k=1}^{n} \left(\overline{Q}_{11}^k \overline{\alpha}_x^k + \overline{Q}_{12}^k \overline{\alpha}_y^k + \overline{Q}_{16}^k \overline{\alpha}_{xy}^k \right) \cdot \left(\overline{h}_k - \overline{h}_{k-1} \right)$$

$$= \Delta T \cdot \sum_{k=1}^{n} \left(\overline{Q}_{11}^k \overline{\alpha}_x^k + \overline{Q}_{12}^k \overline{\alpha}_y^k + \overline{Q}_{16}^k \overline{\alpha}_{xy}^k \right) \cdot \left(h_k - h_{k-1} \right) = N_x^T \tag{3.3}$$

$$\overline{N}_y^T = \Delta T \cdot \sum_{k=1}^{n} \left(\overline{Q}_{12}^k \alpha_x^k + \overline{Q}_{22}^k \alpha_y^k + \overline{Q}_{26}^k \alpha_{xy}^k \right) \cdot \left(\overline{h}_k - \overline{h}_{k-1} \right)$$

$$= \Delta T \cdot \sum_{k=1}^{n} \left(\overline{Q}_{12}^k \alpha_x^k + \overline{Q}_{22}^k \alpha_y^k + \overline{Q}_{26}^k \alpha_{xy}^k \right) \cdot \left(h_k - h_{k-1} \right) = N_y^T \tag{3.4}$$

$$\overline{N}_{xy}^T = \Delta T \cdot \sum_{k=1}^{n} \left(\overline{Q}_{16}^k \alpha_x^k + \overline{Q}_{26}^k \alpha_y^k + \overline{Q}_{66}^k \alpha_{xy}^k \right) \cdot \left(\overline{h}_k - \overline{h}_{k-1} \right)$$

$$= \Delta T \cdot \sum_{k=1}^{n} \left(\overline{Q}_{16}^k \alpha_x^k + \overline{Q}_{26}^k \alpha_y^k + \overline{Q}_{66}^k \alpha_{xy}^k \right) \cdot \left(h_k - h_{k-1} \right) = N_{xy}^T \tag{3.5}$$

$$\overline{M}_x^T = \frac{\Delta T}{2} \cdot \sum_{k=1}^{n} \left(\overline{Q}_{11}^k \alpha_x^k + \overline{Q}_{12}^k \alpha_y^k + \overline{Q}_{16}^k \alpha_{xy}^k \right) \cdot \left(\overline{h}_k^2 - \overline{h}_{k-1}^2 \right)$$

$$= \frac{\Delta T}{2} \cdot \sum_{k=1}^{n} \left(\overline{Q}_{11}^k \alpha_x^k + \overline{Q}_{12}^k \alpha_y^k + \overline{Q}_{16}^k \alpha_{xy}^k \right) \cdot \left(h_k^2 - h_{k-1}^2 \right)$$

$$+ d \cdot \Delta T \cdot \sum_{k=1}^{n} \left(\overline{Q}_{11}^{k} \overline{\alpha}_{x}^{k} + \overline{Q}_{12}^{k} \overline{\alpha}_{y}^{k} + \overline{Q}_{16}^{k} \overline{\alpha}_{xy}^{k} \right) \cdot \left(h_k - h_{k-1} \right)$$

$$\boxed{\overline{M}_{x}^{T} = M_{x}^{T} + d \cdot N_{x}^{T}} \tag{3.6}$$

$$\overline{M}_{y}^{T} = \frac{\Delta T}{2} \cdot \sum_{k=1}^{n} \left(\overline{Q}_{12}^{k} \alpha_{x}^{k} + \overline{Q}_{22}^{k} \alpha_{y}^{k} + \overline{Q}_{26}^{k} \alpha_{xy}^{k} \right) \cdot \left(\overline{h}_{k}^{2} - \overline{h}_{k-1}^{2} \right)$$

$$= \frac{\Delta T}{2} \cdot \sum_{k=1}^{n} \left(\overline{Q}_{12}^{k} \alpha_{x}^{k} + \overline{Q}_{22}^{k} \alpha_{y}^{k} + \overline{Q}_{26}^{k} \alpha_{xy}^{k} \right) \cdot \left(h_{k}^{2} - h_{k-1}^{2} \right)$$

$$+ d \cdot \Delta T \cdot \sum_{k=1}^{n} \left(\overline{Q}_{12}^{k} \alpha_{x}^{k} + \overline{Q}_{22}^{k} \alpha_{y}^{k} + \overline{Q}_{26}^{k} \alpha_{xy}^{k} \right) \cdot \left(h_k - h_{k-1} \right)$$

$$\boxed{\overline{M}_{y}^{T} = M_{y}^{T} + d \cdot N_{y}^{T}} \tag{3.7}$$

$$\overline{M}_{xy}^{T} = \frac{\Delta T}{2} \cdot \sum_{k=1}^{n} \left(\overline{Q}_{16}^{k} \alpha_{x}^{k} + \overline{Q}_{26}^{k} \alpha_{y}^{k} + \overline{Q}_{66}^{k} \alpha_{xy}^{k} \right) \cdot \left(\overline{h}_{k}^{2} - \overline{h}_{k-1}^{2} \right)$$

$$= \frac{\Delta T}{2} \cdot \sum_{k=1}^{n} \left(\overline{Q}_{16}^{k} \alpha_{x}^{k} + \overline{Q}_{26}^{k} \alpha_{y}^{k} + \overline{Q}_{66}^{k} \alpha_{xy}^{k} \right) \cdot \left(h_{k}^{2} - h_{k-1}^{2} \right)$$

$$+ d \cdot \Delta T \cdot \sum_{k=1}^{n} \left(\overline{Q}_{16}^{k} \alpha_{x}^{k} + \overline{Q}_{26}^{k} \alpha_{y}^{k} + \overline{Q}_{66}^{k} \alpha_{xy}^{k} \right) \cdot \left(h_k - h_{k-1} \right)$$

$$\boxed{\overline{M}_{xy}^{T} = M_{xy}^{T} + d \cdot N_{xy}^{T}} \tag{3.8}$$

3.1.3 Overall Force and Moment Resultants

The overall force and moment resultants are obtained by summing the resultants of each laminate about the mid-height of the web. Referring figure 2.1 of chapter 2,

$$\left[N^{T} \right]^{Total} = \left[N^{T} \right]^{TF} + 2 \cdot \left[N^{T} \right]^{WEB} + 2 \cdot \left[N^{T} \right]^{BF} + \left[N^{T} \right]^{BL} \tag{3.9}$$

$$\left[M^{T} \right]^{Total} = \left\{ \left[M^{T} \right] + d\_tf \cdot \left[N^{T} \right] \right\}^{TF} + 2 \cdot \left[M^{T} \right]^{WEB} + 2 \cdot \left\{ \left[M^{T} \right] - d\_bf \cdot \left[N^{T} \right] \right\}^{BF}$$

$$+ \left\{ \left[M^{T} \right] - d\_bl \cdot \left[N^{T} \right] \right\}^{BL} \tag{3.10}$$

3.1.4 Ply Stress Calculation

Ply stresses are obtained using the mid-plane and curvature obtained by multiplying *[abd]* matrix of the equivalent plate formed at the mid-height of the web with the resultants. Mechanical strain is obtained by subtracting the thermal strain from the total strain. Finally, stresses in any ply are obtained by multiplying the ordinary $[\overline{Q}]_k$ matrix with the mechanical strain.

$$\begin{bmatrix} \overline{\varepsilon}_0 \\ \overline{\kappa} \end{bmatrix} = \begin{bmatrix} \overline{a} & \overline{b} \\ \overline{b}^T & \overline{d} \end{bmatrix} \cdot \begin{Bmatrix} [N^T]^{Total} \\ [M^T]^{Total} \end{Bmatrix} \tag{3.11}$$

$$[\varepsilon]_k = [\overline{\varepsilon}^0] + z \cdot [\overline{\kappa}] - [\alpha]_k \cdot \Delta T$$

$$[\sigma]_k = [\overline{Q}]_k \cdot [\varepsilon]_k \tag{3.12}$$

3.2 Finite Element Analysis

Finite element analysis is carried out to validate the present closed form solution. The same hat-section model developed in chapter 2 is used and sole uniform temperature load of 100˚F is applied. The validity of the model confirmed in chapter 2 itself. In addition to the details of the model listed in chapter 2, including material properties, following values of coefficient of thermal expansion are used:

TABLE 3.1

COEFFICIENTS OF THERMAL EXPANSION

AS4/3501-6 Graphite/Epoxy	
Coefficient of Thermal Expansion	Value (in/in/˚F)
Along the Fiber direction (α_1)	-0.5E-6
Transverse to the Fiber direction (α_2)	15E-6

3.3 Results and Discussions

Results of analytical solution are obtained by the code written in MATLAB. On the other hand, finite element results are obtained by ANSYS. The beam with a web angle of 90˚ is used in study to investigate ply stresses due to thermal loading. For angle plies in laminated composites, the dominate stresses are the shear stresses (τ_{xy}) and the secondary stresses are the stresses in y-direction (σ_y). Due to the negligible coefficient of thermal expansion along the fiber direction, the values of stresses along x-direction (σ_x) were observed to be insignificant. Hence, they are not used in the comparison. For a 0˚ ply, the dominate stress is observed to be in y-direction (σ_y). Ply stresses of FEM model are obtained by taking average of nodal values of elements located far from the constrained area. Figure 3.1 shows FEM contour plot of shear stresses in top plies of hat-cross section composite beam for applied uniform temperature of 100˚F.

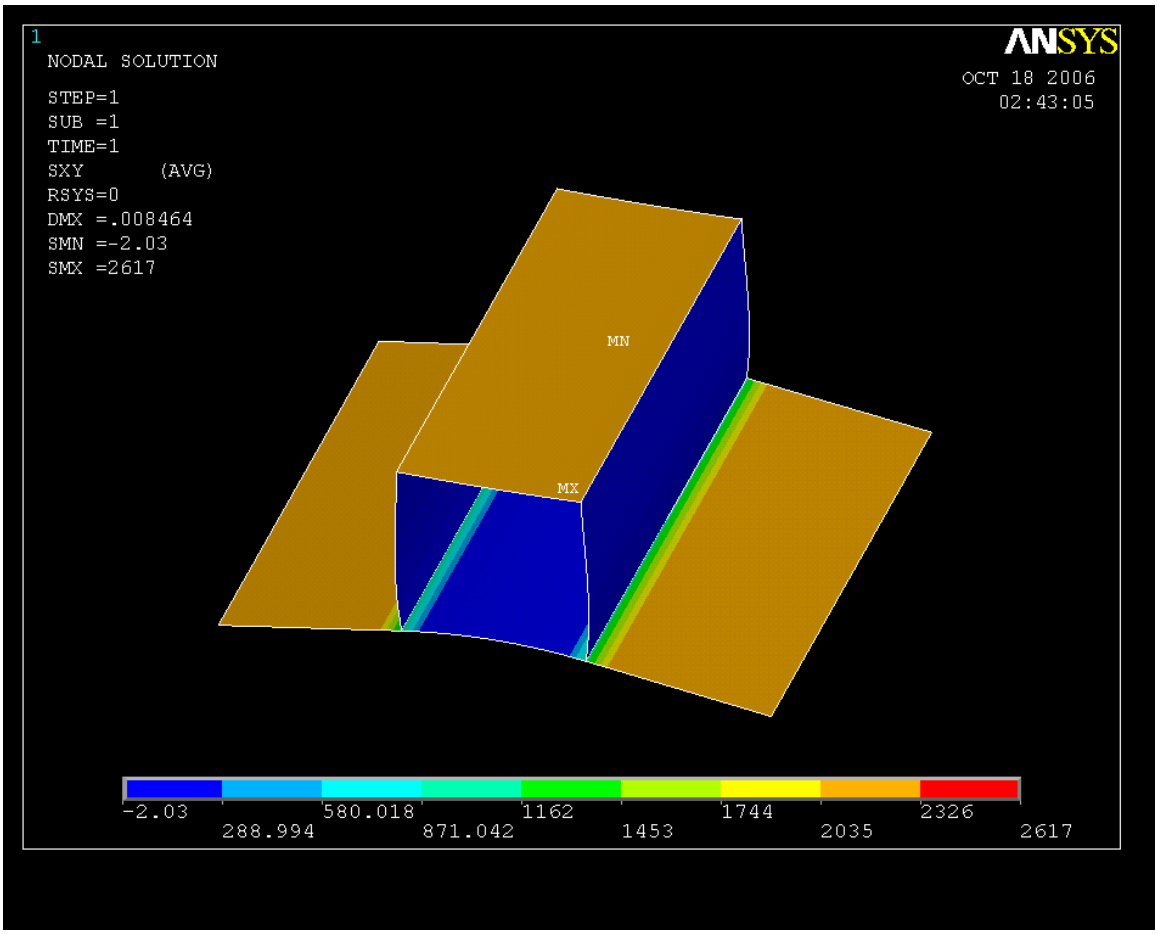

Figure 3.1 Contour Plot of τ_{xy} in Top Plies

Table 3.2 lists the comparison of shear stress values obtained from FEM and present method. As seen in the table, shear stresses are dominant in angle plies; on the other hand, they have null value for 0˚ ply. Excellent conformity was observed between FEM and present method.

TABLE 3.2

COMPARISON OF SHEAR STRESSES BETWEEN FEM AND PRESENT METHOD FOR BOTTOM FLANGE LAMINATE

	Layer	FEM Results τ_{xy} (psi)	Present Method τ_{xy} (psi)	% Error
45	Top	2128.5	2161.0	-1.5 %
	Bottom	2128.2	2160.7	-1.5 %
-45	Top	-2136.3	-2160.7	-1.1 %
	Bottom	-2134.6	-2160.4	-1.2 %
-45	Top	-2134.6	-2160.4	-1.2 %
	Bottom	-2132.8	-2160.1	-1.3 %
45	Top	2127.7	2160.1	-1.5 %
	Bottom	2127.4	2159.8	-1.5 %
0	Top	0.0	0.0	0.0 %
	Bottom	0.0	0.0	0.0 %
0	Top	0.0	0.0	0.0 %
	Bottom	0.0	0.0	0.0 %
45	Top	2126.9	2159.2	-1.5 %
	Bottom	2126.6	2158.9	-1.5 %
-45	Top	-2126.1	-2158.9	-1.5 %
	Bottom	-2124.4	-2158.6	-1.6 %
-45	Top	-2124.4	-2158.6	-1.6 %
	Bottom	-2122.7	-2158.3	-1.7 %

TABLE 3.2 - Continued

45	Top	2126.1	2158.3	-1.5 %
	Bottom	2125.8	2158.0	-1.5 %

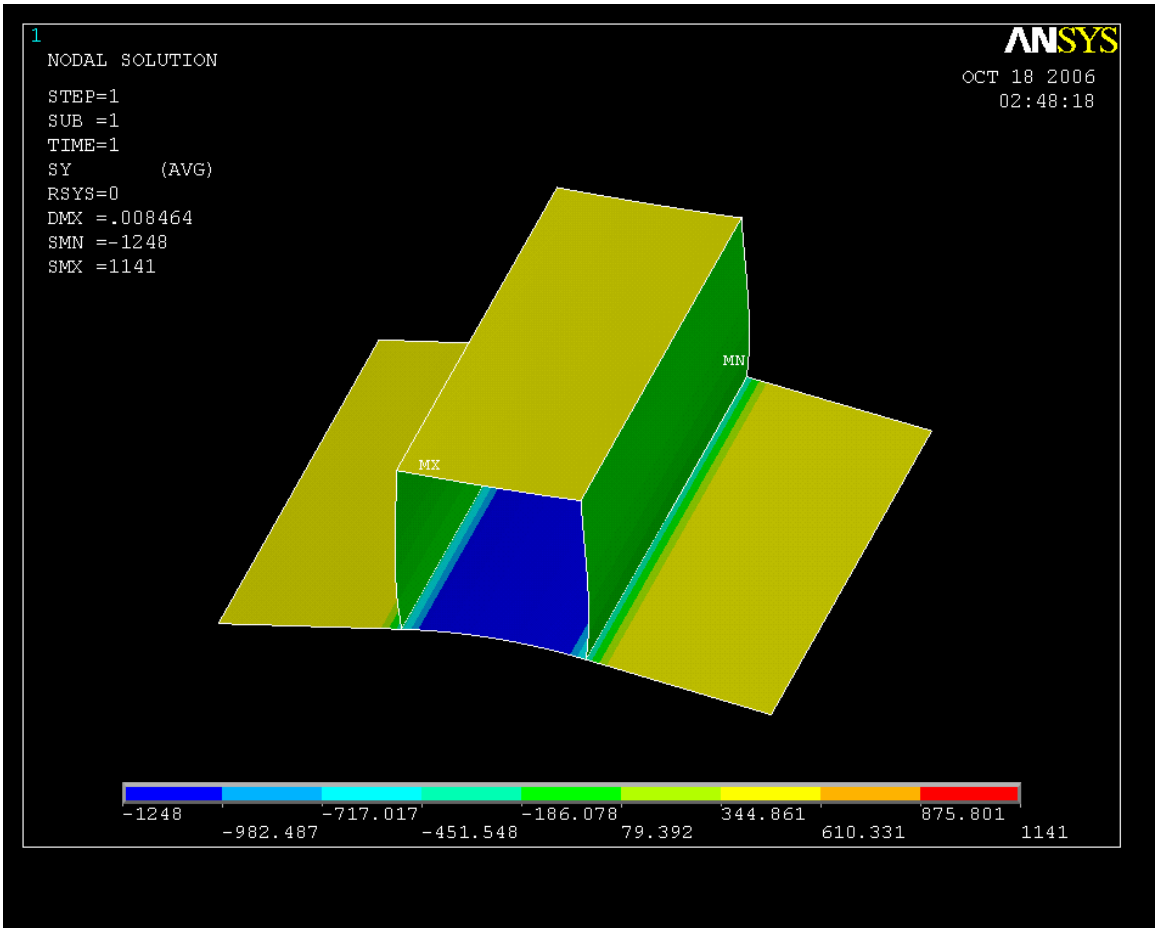

Figure 3.2 Contour Plot of σ_y in Top Plies

The stresses in y-direction (σ_y) are observed to have significant value for angle plies and these stresses are dominant for 0˚ ply. Figure 3.2 gives a pictorial representation of σ_y stresses in top plies of the cross-section. Excellent agreement was

observed in the values obtained for 0˚ ply. However, in angle plies, the difference seems to be high. This may be due to the effect of edge constraint of the laminate.

TABLE 3.3

COMPARISON OF σ_y STRESSES BETWEEN FEM AND PRESENT METHOD FOR BOTTOM FLANGE LAMINATE

	Layer	FEM Results σ_y (psi)	Present Method σ_y (psi)	% Error
45	Top	445.4	511.6	-14.9 %
	Bottom	445.4	511.0	-14.7 %
-45	Top	452.6	511.0	-12.9 %
	Bottom	451.4	510.4	-13.1 %
-45	Top	451.4	510.4	-13.1 %
	Bottom	450.1	509.8	-13.2 %
45	Top	445.5	509.8	-14.4 %
	Bottom	445.5	509.2	-14.2 %
0	Top	-1783.7	-1763.5	1.1 %
	Bottom	-1783.8	-1763.7	1.1 %
0	Top	-1783.6	-1763.7	1.1 %
	Bottom	-1783.9	-1763.9	1.1 %
45	Top	445.6	508.0	-14.0 %
	Bottom	445.7	507.4	-14.0 %
-45	Top	445.2	507.4	-14.0 %
	Bottom	444.0	506.8	-14.1 %

TABLE 3.3 - Continued

-45	Top	444.0	506.8	-14.1 %
	Bottom	442.7	506.1	-14.3 %
45	Top	445.7	506.1	-13.6 %
	Bottom	445.8	505.5	-13.4 %

CHAPTER 4

EVALUATION OF CENTROID AND SHEAR CENTER

The location of centroid and shear center in a thin-walled laminated composite, closed-section beam is a function of the geometry and the material properties of the section. For isotropic material, by definition, centroid is located such that an axial load does not cause a change in curvature and a bending moment does not produce axial strain. Likewise, shear forces acting at the shear center do not cause twist. In other words, centroid decouples axial extension and bending, where as, shear center decouples bending and twisting, mechanisms of a beam. However, composite material exhibit unique structural coupling characteristic. For a composite beam subjected to axial force at centroid there exists an extension/twist coupling and for applied pure bending moment there exists a bending/twisting coupling. That is, the beam may also twist when subjected to such loads.

In general, extension/twist coupling is obtained in beams with antisymmetric lay-up, while bending/twist coupling is obtained in beams with symmetric lay-up configuration. In section 4.1, centroid and shear center are evaluated based on the extensional application of analytical solution developed in chapter 2.

4.1 Centroid and Shear Center

Determining the location of centroid and shear center plays an important role in the engineering analysis. The methodology developed to determine these locations is

first applied to a closed cross section with varying web angles. After validating the results with isotropic material and observing the behavior for symmetric and anti-symmetric laminate, the methodology is applied to the hat cross-section.

4.1.1 Geometry of Closed Cross-Section

Box cross-section is divided into individual laminates. As shown in Figure 4.1, let b_{tf} be the width of top flange, b_{bf} is the width of bottom flange, t_{ply} is the thickness of each ply, b_w is the width of webs and H is the vertical height between the middle of top and bottom laminates. It should be noted that b_{tf} and H are kept constant, where as b_w and b_{bf} varies according to web angle, $\sin^{-1}(H/b_w)$. Hence, b_{bf} is dependent of the angle. Also, for web angle of 90˚, the box becomes a square cross section of unit dimensions.

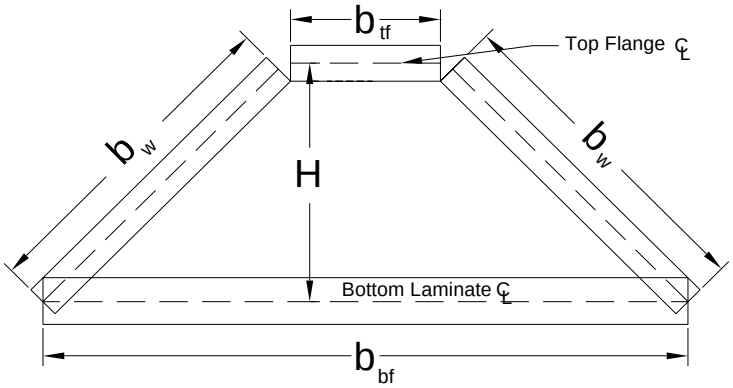

Figure 4.1 Geometry of box cross-section

4.1.2 The Procedure of the Approach

In this section, the methodology developed for the determination of centroid and shear center is presented.

4.1.2.1 Centroid

The centroid is located such that the beam's axis remains straight when an axial force is applied at the centroid. Although this axis remains straight, the beam may twist about the axis of twist [5].

Recalling equation 2.20, we have

$$\begin{bmatrix} \bar{\varepsilon}_x^o \\ \bar{\kappa}_x \end{bmatrix} = \begin{Bmatrix} \bar{a}_{11} & \bar{b}_{11} \\ \bar{b}_{11} & \bar{d}_{11} \end{Bmatrix} \begin{bmatrix} \overline{N}_x \\ \overline{M}_x \end{bmatrix}$$

According to the definition of the "neutral" plane, $\bar{\varepsilon}_x^0$ depends only on $\overline{N}_x$ and $\bar{\kappa}_x$ depends only on $\overline{M}_x$. Therefore, for applied pure moment, $\overline{N}_x = 0$, hence equation 2.20 reduces to,

$$\bar{\varepsilon}_x^0 = \bar{b}_{11} \cdot \overline{M}_x \text{ and } \bar{\kappa}_x = \bar{d}_{11} \cdot \overline{M}_x \tag{3.1}$$

from equation 2.3, strain at any location is given as

$$\bar{\varepsilon}_x = \bar{\varepsilon}_0 + \bar{z}_c \cdot \bar{\kappa}_x$$

Substituting equation 3.1 in above equation and $\bar{\varepsilon}_x$ must be equal to zero at neutral plane. Thus, we write

$$\bar{\varepsilon}_x = \bar{\varepsilon}_0 + \bar{z}_c \cdot \bar{\kappa}_x = 0$$

$$\Rightarrow (\bar{b}_{11} + \bar{d}_{11} \cdot \bar{z}_c) \cdot \overline{M}_x = 0 \qquad (\Theta\ \overline{M}_x \neq 0)$$

$$\boxed{\bar{z}_c = -\frac{\bar{b}_{11}}{\bar{d}_{11}}} \tag{3.2}$$

Where, $\bar{b}_{11}$ and $\bar{d}_{11}$ are evaluated at the chosen reference plane, which is the mid-height of the web.

4.1.2.2 Shear Center

Shear center is defined such that transverse load acting at the shear center of an orthotropic beam does not cause twist. In thin-walled, closed-section beams the torque due to the induced twist moment is small compared with the torque due to the induced shear force. In the following we neglect the twist moment [5].

From chapter 2, for closed-section beams, equation 2.18 can be written as,

$$\begin{bmatrix} \bar{\gamma}^{o}_{xy} \\ \bar{\kappa}_{xy} \end{bmatrix} = \begin{Bmatrix} \bar{a}_{66} & \bar{b}_{66} \\ \bar{b}_{66} & \bar{d}_{66} \end{Bmatrix} \cdot \begin{bmatrix} \bar{N}_{xy} \\ \bar{M}_{xy} \end{bmatrix} \tag{3.3}$$

According to the definition of the "torque neutral" surface, $\bar{\gamma}^{0}_{xy}$ depends only of $\bar{N}_{xy}$ and $\bar{\kappa}_{xy}$ depends only on $\bar{M}_{xy}$. Therefore, for applied torque, $\bar{N}_{xy}$ = 0, hence equation 3.3 reduces to,

$$\bar{\gamma}^{0}_{xy} = \bar{b}_{66} \cdot \bar{M}_{xy} \quad \text{and} \quad \bar{\kappa}_{xy} = \bar{d}_{66} \cdot \bar{M}_{xy} \tag{3.4}$$

from equation 2.3, shear strain at any location is given as

$$\bar{\gamma}_{xy} = \bar{\gamma}^{0}_{xy} + \bar{z}_{sc} \cdot \bar{\kappa}_{xy} \tag{3.5}$$

Substituting equation 3.4 in equation 3.5 and $\bar{\gamma}_{xy}$ must be equal to zero at torque neutral plane. Thus, we write

$$\bar{\gamma}_{xy} = \bar{\gamma}^{0}_{xy} + \bar{z}_{sc} \cdot \bar{\kappa}_{xy} = 0$$

$$\Rightarrow (\bar{b}_{66} + \bar{d}_{66} \cdot \bar{z}_{sc}) \cdot \overline{M}_{xy} = 0 \qquad \left(\Theta\ \overline{M}_{xy} \neq 0\right)$$

$$\boxed{\bar{z}_{sc} = -\frac{\bar{b}_{66}}{\bar{d}_{66}}} \qquad (3.5)$$

Where, $\bar{b}_{66}$ and $\bar{d}_{66}$ are evaluated at the chosen reference plane, which is the mid-height of the web.

4.1.3 Verification of the Present Approach

The approach is verified in two ways: one is by comparing the results of an isotropic cross-section of aluminum material and the also by observing the results of composite cross-section for symmetric and unsymmetric cases. Data and dimension of the model are shown in table 4.1.

TABLE 4.1

MATERIAL PROPERTIES AND DIMENSIONS OF THE ISOTROPIC MODEL

Name	**Values**
Elastic Modulus, E (psi)	10E+06
Poisson's Ratio, ν	0.33
Widths, b_{tf} and b_{bf} (in)	1
Thickness, t_{tf}, t_{bf}, and t_w (in)	0.03, 0.03, and 0.02 respectively
Web Height, H (in)	1

The dimensions of the cross-section are shown in figure 4.1 and the web angle is varied at 15 degrees ranging from 30˚ to 90˚. It should be noted that for a web angle of 90˚ the cross-section is doubly symmetrical, and both the centroid and the shear center

coincide with the center of the cross section. For other web angles, the cross-section becomes singly symmetrical; hence the centroid and shear center will lie along the symmetric y-axis and the y-coordinates as listed in table 4.2.

TABLE 4.2

COMPARISON BETWEEN CONVENTIONAL AND PRESENT APPROACH FOR CLOSED CROSS SECTIONS MADE OF ISOTROPIC MATERIAL

	Neutral Axis Location from Mid-plane of Bottom Laminate			Torque Neutral Axis Location from Mid-plane of Bottom Laminate		
Web Angle, θ	Convention-al Method (in)	Present Method (in)	% Error	Convention-al Method (in)	Present Method (in)	% Error
90˚	0.500	0.500	0.0 %	0.500	0.500	0.0 %
75˚	0.432	0.434	-0.6 %	0.375	0.398	-6.3 %
60˚	0.377	0.380	-0.8 %	0.325	0.337	-3.8 %
45˚	0.330	0.332	-0.4 %	0.309	0.298	3.6 %
30˚	0.287	0.287	-0.1 %	0.290	0.268	7.6 %

4.2 Present Approach Applied to Closed Composite Cross-Section

Two cases are studied for composite cross-sections. The material used in this study was AS4/3501 graphite epoxy laminates. Its properties are listed in table 2.4 of chapter 2.

Case 1: Symmetric Lay-up

A closed thin-walled composite beam with orthotropic and symmetrical lay-up behaves similarly to an isotropic beam [5]. The geometry and lay-up sequence used to study composite beam is shown in figure 4.2. It should be noted that for a web angle of 90˚, the beam becomes square cross-section with unit dimensions as shown in figure 4.2, for which the centroid and shear center will coincide with the center of the cross-section. The centroid and shear center will lie along the symmetric z-axis of the cross-sections; table 4.3 lists the location of z-coordinate of neutral and torque neutral axis.

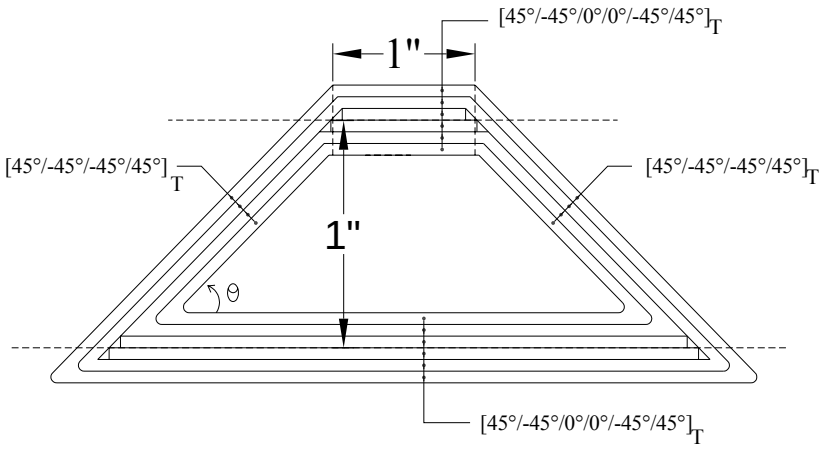

Figure 4.2 Geometry and Lay-up Sequence of Symmetric Composite Sections

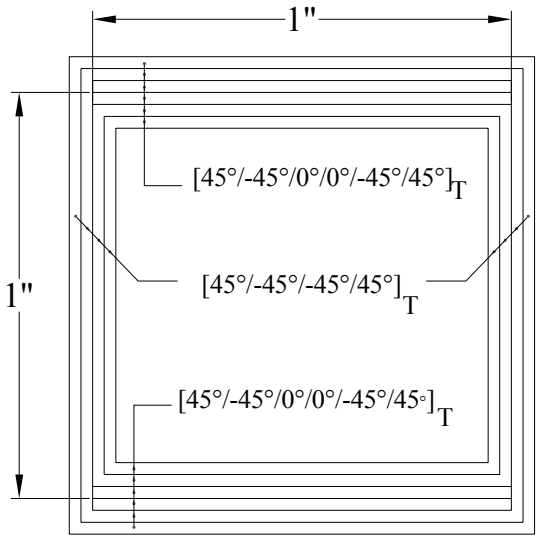

Figure 4.3 Composite Cross-Section for 90˚ Web Angle

TABLE 4.3

PRESENT APPROACH APPLIED TO CLOSED CROSS SECTION SYMMETRIC LAY-UP COMPOSITE BEAMS

Web Angle, θ	Neutral Axis Location from Mid-plane of Bottom Laminate (in)	Torque Neutral Axis Location from Mid-plane of Bottom Laminate (in)
90˚	0.500	0.500
75˚	0.398	0.439
60˚	0.328	0.388
45˚	0.273	0.346
30˚	0.223	0.308

Case 2: Bottom Unsymmetric Lay-up

The bottom laminate is kept unsymmetric to study its effect on the location of centroid and shear center for the geometries studied in case 1. The geometry and lay-up sequence are shown in figure 4.4. From table 4.4, it was observed that the

shear center and centroid does not coincide with the center of cross-section of the beam for the web angle of 90˚ for which the geometry of cross-section is symmetric about the both the axis.

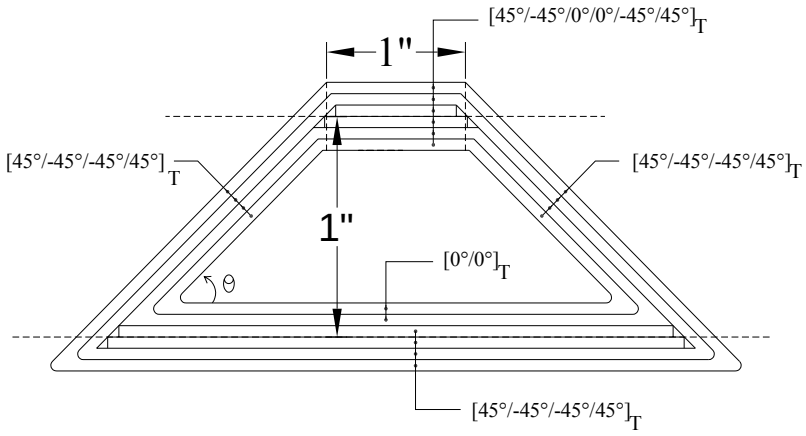

Figure 4.4 Geometry and Lay-up Sequence of Unsymmetric Composite Sections

TABLE 4.4

PRESENT APPROACH APPLIED TO CLOSED CROSS SECTION
UNSYMMETRIC LAY-UP COMPOSITE BEAMS

Web Angle, θ	Neutral Axis Location from Mid-plane of Bottom Laminate (in)	Torque Neutral Axis Location from Mid-plane of Bottom Laminate (in)
90˚	0.497	0.501
75˚	0.394	0.440
60˚	0.324	0.390
45˚	0.269	0.348
30˚	0.219	0.310

4.3 Present Approach Applied to Hat Sectioned Composite Beam

Finally, the centroid and shear center of hat-cross section composite beams with the geometry and lay-up sequence shown in figure 2.8 and with the material properties given in chapter 2 are investigated. Table 4.5 lists the values:

TABLE 4.5

PRESENT APPROACH APPLIED TO HAT CROSS SECTION COMPOSITE BEAMS

Web Angle, θ	Neutral Axis Location from Mid-plane of Bottom Laminate (in)	Torque Neutral Axis Location from Mid-plane of Bottom Laminate (in)
90˚	0.244	0.267
75˚	0.221	0.251
60˚	0.204	0.240
45˚	0.189	0.233
30˚	0.174	0.232

CHAPTER 5

CONCLUSION AND RECOMMENDATION

A simple analytical method for analyzing composite beams with hat-section is presented. The current model includes the effect of induced in-plane deformation due to bending for an unsymmetrical cross-section while the conventional analysis using the smeared mechanical properties of laminate ignores this coupling effect. Finite element analysis was conducted to obtain the results for comparison. It is concluded that the axial and bending stiffness obtained by the present method give an excellent agreement with the finite element results. However, the results obtained by the conventional method in axial load case give significant differences from the finite element results.

The stiffness matrices obtained using the developed method is extended for thermal analysis. A simple closed form solution is developed to obtain ply stresses due to thermal loading. Results were validated and excellent agreement is observed with the finite element calculation. Based on the stiffness matrices obtained, a simple methodology is developed to determine the location of centroid and shear center for a closed cross-section. Results are validated by comparing with isotropic materials and also by observing the behavior of composite material for symmetric and anti-symmetric cases.

It is concluded that with the present method, analysis of hat-section reinforced composite beams can easily be performed with significant accuracy. The developed tool

is handy in providing the parametric study for composite structural design.

For the usage of the closed form expression of the stiffness matrices, a full model test is necessary to validate the developed model and to investigate the failure mechanism of the laminate. The response of structure due to combined loading such as mechanical and thermal, force and moment, moment and torque etc. is also an interesting area to study. Stiffnesses and thermal response of other cross-sections such as I-section, J-section, C-section, Triangular section, Honey-comb cross-section etc. can also be investigate using approach developed in this dissertation. However, at least one new such cross-section geometry should to be validated with finite element analysis and experimental testing. Further, the approach can be extended for the analysis of bridge structures. Hence, the present method can provide a generic solution to various cross-sectional beams.

APPENDIX A

STIFFNESS MATRIX TRANSFORMATION EQUATIONS

A.1 Stress-Strain relationship

According to Hooke's law, the linear elastic stress-strain constitutive relationship in material and global coordinates are given as

$$\begin{aligned} [\sigma]_{1-2} &= [Q_{1-2}] \cdot [\varepsilon]_{1-2} \\ [\bar{\sigma}]_{x-y} &= [\bar{Q}_{x-y}] \cdot [\bar{\varepsilon}]_{x-y} \end{aligned} \tag{A.1}$$

Where,

$$[\sigma]_{1-2} = \begin{bmatrix} \sigma_1 \\ \sigma_2 \\ \tau_{12} \end{bmatrix} \quad \text{and} \quad [\bar{\sigma}]_{x-y} = \begin{bmatrix} \sigma_x \\ \sigma_y \\ \tau_{xy} \end{bmatrix} \tag{A.2}$$

$$[\varepsilon]_{1-2} = \begin{bmatrix} \varepsilon_1 \\ \varepsilon_2 \\ \gamma_{12} \end{bmatrix} \quad \text{and} \quad [\bar{\varepsilon}]_{x-y} = \begin{bmatrix} \varepsilon_x \\ \varepsilon_y \\ \gamma_{xy} \end{bmatrix} \tag{A.3}$$

The subscripts, 1 and 2 refer to the material coordinate system, x and y refer to global coordinate system, $[Q_{1-2}]$ and $[\bar{Q}_{x-y}]$ are the stiffness matrices of zero degree ply with respect to 1-2 and x-y coordinate system, respectively. Stress-strain relationship in global coordinate is obtained using transformation matrices given in section A.2.

A.2 Transformation Matrices

In this section stress and strain transformation matrices for x-axis rotation and z-axis rotation are listed.

A.2.1 Stress Transformation Matrices

Rotated θ about x axis

3D stress transformation matrix rotated a positive angle θ about x-axis is given as

$$[T_\sigma(\theta)]_x^{3D} = \begin{bmatrix} 1 & 0 & 0 & 0 & 0 & 0 \\ 0 & c_x^{\,2} & s_x^{\,2} & 2s_x c_x & 0 & 0 \\ 0 & s_x^{\,2} & c_x^{\,2} & -2s_x c_x & 0 & 0 \\ 0 & -s_x c_x & s_x c_x & c_x^{\,2} - s_x^{\,2} & 0 & 0 \\ 0 & 0 & 0 & 0 & c_x & -s_x \\ 0 & 0 & 0 & 0 & s_x & c_x \end{bmatrix} \tag{A.4}$$

Where $c_x = \cos\theta$ and $s_x = \sin\theta$

For plane stress condition, 6x6 stress transformation matrix reduces to 3x3 matrix, obtained by crossing out the 3rd, 4th and 5th rows and columns of the $[T_\sigma(\theta)]_x^{3D}$ matrix. Therefore,

$$[T_\sigma(\theta)]_x = \begin{bmatrix} 1 & 0 & 0 \\ 0 & c_x^{\,2} & 0 \\ 0 & 0 & c_x \end{bmatrix} = [T_\sigma(-\theta)]_x^T \tag{A.5}$$

Rotated β about z axis

3D stress transformation matrix rotated a positive angle β about z-axis is given as

$$[T_\sigma(\beta)]_x^{3D} = \begin{bmatrix} c_z^2 & s_z^2 & 0 & 0 & 0 & 2c_z s_z \\ s_z^2 & c_z^{\,2} & 0 & 0 & 0 & -2c_z s_z \\ 0 & 0 & 1 & 0 & 0 & 0 \\ 0 & 0 & 0 & c_z & -s_z & 0 \\ 0 & 0 & 0 & s_z & c_z & 0 \\ -c_z s_z & c_z s_z & 0 & 0 & 0 & c_z^2 - s_z^2 \end{bmatrix} \tag{A.6}$$

Where $c_z = \cos\beta$ and $s_z = \sin\beta$

2D stress transformation matrix about z-axis is written as

$$[T_\sigma(\beta)]_z = \begin{bmatrix} c_z^2 & s_z^2 & 2c_z s_z \\ s_z^2 & c_z^2 & -2c_z s_z \\ -c_z s_z & c_z s_z & c_z^2 - s_z^2 \end{bmatrix} \tag{A.7}$$

Also,

$$[T_\sigma(-\beta)]_z^T = \begin{bmatrix} c_z^2 & s_z^2 & c_z s_z \\ s_z^2 & c_z^2 & -c_z s_z \\ -2c_z s_z & 2c_z s_z & c_z^2 - s_z^2 \end{bmatrix} \tag{A.8}$$

A.2.2 Strain Transformation

Rotated θ about x axis

3D strain transformation matrix rotated a positive angle θ about x-axis is given as

$$[T_\varepsilon(\theta)]_x^{3D} = \begin{bmatrix} 1 & 0 & 0 & 0 & 0 & 0 \\ 0 & c_x^2 & s_x^2 & c_x s_x & 0 & 0 \\ 0 & s_x^2 & c_x^2 & -c_x s_x & 0 & 0 \\ 0 & -2c_x s_x & 2c_x s_x & c_x^2 - s_x^2 & 0 & 0 \\ 0 & 0 & 0 & 0 & c_x & -s_x \\ 0 & 0 & 0 & 0 & s_x & c_x \end{bmatrix} \tag{A.9}$$

2D strain transformation matrix about x-axis is written as

$$[T_\varepsilon(\theta)]_x = \begin{bmatrix} 1 & 0 & 0 \\ 0 & c_x{}^2 & 0 \\ 0 & 0 & c_x \end{bmatrix} = [T_\sigma(-\theta)]_x^T \tag{A.10}$$

Rotated β about z axis

3D strain transformation matrix rotated a positive angle β about z-axis is given as

$$[T_\varepsilon(\beta)]_z = \begin{bmatrix} c_z^2 & s_z^2 & 0 & 0 & 0 & c_z s_z \\ s_z^2 & c_z^2 & 0 & 0 & 0 & -c_z s_z \\ 0 & 0 & 1 & 0 & 0 & 0 \\ 0 & 0 & 0 & c_z & -s_z & 0 \\ 0 & 0 & 0 & s_z & c_z & 0 \\ -2c_z s_z & 2c_z s_z & 0 & 0 & 0 & c_z^2 - s_z^2 \end{bmatrix}$$

2D strain transformation matrix about x-axis is written as

$$\left[T_{\varepsilon}(\beta)\right]_z = \begin{bmatrix} c_z^2 & s_z^2 & c_z s_z \\ s_z^2 & c_z^2 & -c_z s_z \\ -2c_z s_z & 2c_z s_z & c_z^2 - s_z^2 \end{bmatrix} = \left[T_{\sigma}(-\beta)\right]_z^T \tag{A.11}$$

A.3 Transformation of stress and strain from material coordinate system to laminate coordinate system

The stress and strain transformations from the global coordinate to the material coordinate are given as

$$\begin{aligned} \left[\sigma\right]_{1-2} &= \left[T_{\sigma}\right] \cdot \left[\bar{\sigma}\right]_{x-y} \\ \left[\varepsilon\right]_{1-2} &= \left[T_{\varepsilon}\right] \cdot \left[\bar{\varepsilon}\right]_{x-y} \end{aligned} \tag{A.12}$$

Rewriting equation A.12, we have

$$\begin{aligned} \left[\bar{\sigma}\right]_{x-y} &= \left[T_{\sigma}\right]^{-1} \cdot \left[\sigma\right]_{1-2} \\ \left[\bar{\varepsilon}\right]_{x-y} &= \left[T_{\varepsilon}\right]^{-1} \cdot \left[\varepsilon\right]_{1-2} \end{aligned} \tag{A.13}$$

A.4 General Transformation equation of stiffness matrix from material to global coordinate system

Using equations A.13, A.1 and A.12, we have

$$\begin{aligned} \left[\bar{\sigma}\right]_{x-y} &= \left[T_{\sigma}\right]^{-1} \cdot \left[\sigma\right]_{1-2} = \left[T_{\sigma}\right]^{-1} \cdot \left[Q\right] \cdot \left[\varepsilon\right]_{1-2} \\ \left[\bar{\sigma}\right]_{x-y} &= \left[T_{\sigma}\right]^{-1} \cdot \left[Q\right] \cdot \left[T_{\varepsilon}\right] \cdot \left[\bar{\varepsilon}\right]_{x-y} \end{aligned} \tag{A.14}$$

Comparing equations A.14 and A.1, stiffness transformation matrix is,

$$\left[\bar{Q}_{x-y}\right] = \left[T_{\sigma}\right]^{-1} \cdot \left[Q\right] \cdot \left[T_{\varepsilon}\right] \tag{A.15}$$

A.5 Stiffness Transformation matrix for θ rotation about x-axis

Stress-strain relationship in global coordinate is given as

$$[\bar{\sigma}]_{x-y} = [\bar{Q}] \cdot [\bar{\varepsilon}]_{x-y}$$

Where,

$$\left[\hat{Q}\right] = [T_\sigma(-\theta)]_x \cdot [Q] \cdot [T_\varepsilon(\theta)]_x \qquad \left([T_\sigma(\theta)]^{-1} = [T_\sigma(-\theta)]\right)$$

$$\left[\hat{Q}\right] = [T_\sigma(-\theta)]_x \cdot [Q] \cdot [T_\sigma(-\theta)]_x^T \qquad \left([T_\varepsilon(\theta)]_x = [T_\sigma(-\theta)]_x^T\right)$$

$$\left[\hat{Q}\right] = \begin{bmatrix} 1 & 0 & 0 \\ 0 & c_x{}^2 & 0 \\ 0 & 0 & c_x \end{bmatrix} \cdot \begin{bmatrix} Q_{11} & Q_{12} & 0 \\ Q_{12} & Q_{22} & 0 \\ 0 & 0 & Q_{66} \end{bmatrix} \cdot \begin{bmatrix} 1 & 0 & 0 \\ 0 & c_x{}^2 & 0 \\ 0 & 0 & c_x \end{bmatrix}$$

$$\left[\hat{Q}\right] = \begin{bmatrix} \hat{Q}_{11} & \hat{Q}_{12} & \hat{Q}_{16} \\ \hat{Q}_{12} & \hat{Q}_{22} & \hat{Q}_{26} \\ \hat{Q}_{16} & \hat{Q}_{26} & \hat{Q}_{66} \end{bmatrix}$$

Where,

$$\hat{Q}_{11} = Q_{11}$$

$$\hat{Q}_{21} = \hat{Q}_{12} = c_x^2 Q_{12}$$

$$\hat{Q}_{22} = c_x^4 Q_{22} \qquad \text{(A.16)}$$

$$\hat{Q}_{66} = c_x^2 Q_{66}$$

and, $\hat{Q}_{16} = \hat{Q}_{61} = \hat{Q}_{26} = \hat{Q}_{62} = 0$

A.6 Stiffness Transformation matrix for β rotation about z-axis

Modified stiffness matrix for first rotating angle θ about x-axis and then β about z-axis is written as,

$$\left[\bar{Q}^{"}\right] = [T_\sigma(-\beta)]_z \cdot \left[\hat{Q}\right] \cdot [T_\sigma(-\beta)]_z^T$$

$$\left[\overline{Q}''\right]=\begin{bmatrix} c_z^2 & s_z^2 & 2c_z s_z \\ s_z^2 & c_z^2 & -2c_z s_z \\ -c_z s_z & c_z s_z & c_z^2 - s_z^2 \end{bmatrix}\cdot\begin{bmatrix} \hat{Q}_{11} & \hat{Q}_{12} & \hat{Q}_{16} \\ \hat{Q}_{12} & \hat{Q}_{22} & \hat{Q}_{26} \\ \hat{Q}_{16} & \hat{Q}_{26} & \hat{Q}_{66} \end{bmatrix}\cdot\begin{bmatrix} c_z^2 & s_z^2 & c_z s_z \\ s_z^2 & c_z^2 & -c_z s_z \\ -2c_z s_z & 2c_z s_z & c_z^2 - s_z^2 \end{bmatrix}$$

$$\left[\overline{Q}''\right]=\begin{bmatrix} \overline{Q}_{11}'' & \overline{Q}_{12}'' & \overline{Q}_{16}'' \\ \overline{Q}_{12}'' & \overline{Q}_{22}'' & \overline{Q}_{26}'' \\ \overline{Q}_{16}'' & \overline{Q}_{26}'' & \overline{Q}_{66}'' \end{bmatrix}$$

Where,

$$\overline{Q}_{11}'' = c_z^4 Q_{11} + 2s_z^2 c_z^2 (c_x^2 Q_{12} + 2c_x^2 Q_{66}) + s_z^4 c_x^4 Q_{22}$$

$$\overline{Q}_{22}'' = s_z^4 Q_{11} + 2s_z^2 c_z^2 (c_x^2 Q_{12} + 2c_x^2 Q_{66}) + c_z^4 c_x^4 Q_{22}$$

$$\overline{Q}_{12}'' = s_z^2 c_z^2 (Q_{11} + c_x^4 Q_{22} - 4c_x^2 Q_{66}) + (s_z^4 + c_z^4) c_x^2 Q_{12} \qquad \text{(A.17)}$$

$$\overline{Q}_{16}'' = s_z c_z^3 (Q_{11} - c_x^2 Q_{12} - 2c_x^2 Q_{66}) + s_z^3 c_z (c_x^2 Q_{12} - c_x^4 Q_{22} + 2c_x^2 Q_{66})$$

$$\overline{Q}_{26}'' = c_z s_z^3 (Q_{11} - c_x^2 Q_{12} - 2c_x^2 Q_{66}) + c_z^3 s_z (c_x^2 Q_{12} - c_x^4 Q_{22} + 2c_x^2 Q_{66})$$

$$\overline{Q}_{66}'' = s_z^2 c_z^2 (Q_{11} + c_x^4 Q_{22} - 2c_x^2 Q_{12} - 2c_x^2 Q_{66}) + (s_z^4 + c_z^4) c_x^2 Q_{66}$$

A.7 Transformation matrix for coefficient of thermal expansion

$$\left[\overline{\alpha}\right]_{x-y} = [T_\varepsilon]_z^{-1} \cdot [T_\varepsilon]_x^{-1} \cdot [\varepsilon]_{1-2}$$

$$\overline{\alpha}_{xx} = c_z^2 \alpha_{11} + s_z^2 c_x^2 \alpha_{22} - c_z s_z c_x \alpha_{12}$$

$$\overline{\alpha}_{yy} = s_z^2 \alpha_{11} + c_z^2 c_x^2 \alpha_{22} + c_z s_z c_x \alpha_{12} \qquad \text{(A.18)}$$

$$\overline{\alpha}_{xy} = 2c_z s_z \left(\alpha_{11} - c_x^2 \alpha_{22}\right) + \left(c_z^2 - s_z^2\right) \cdot c_x \alpha_{12}$$

APPENDIX B

CURVATURE CALCULATIONS (11)

This section describes how to obtain curvature from the deflected curved shape of the beam. The obtained curvature and the applied moment will be used to compute the bending rigidity of the beam. Any three points selected on the same line can be used to determine the curvature of this line by geometrical calculations. Points A, B, and C in Figure B.1 represent these arbitrary points used for the curvature calculation and their coordinates are (x_1,y_1), (x_2,y_2) and (x_3,y_3), respectively.

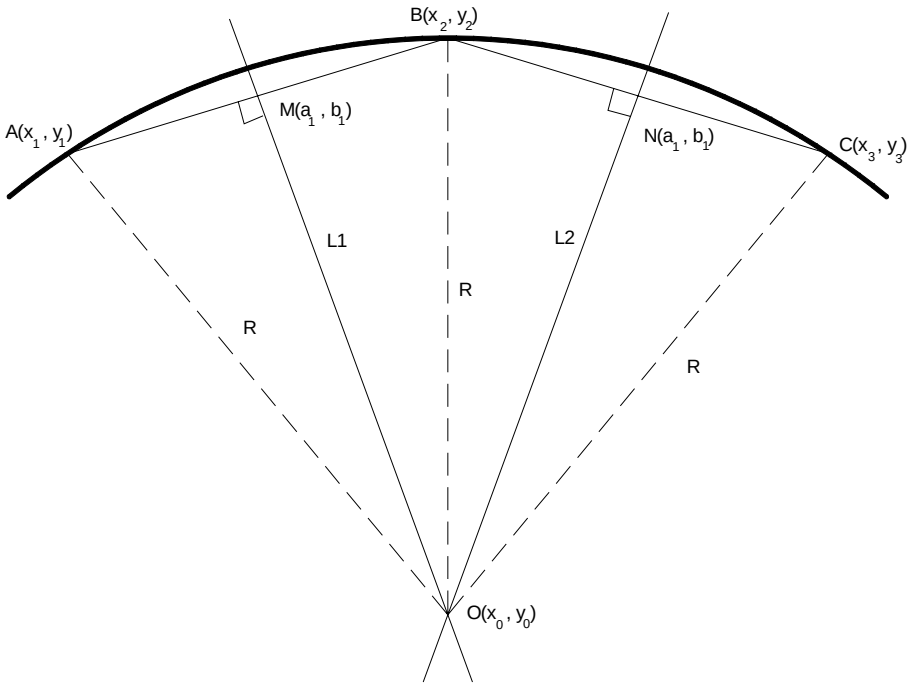

Figure B.1. Geometrical representation of the curvature calculation

Using x and y coordinates of the points A and B, slope and center point of the line AB can be defined, as shown below:

$$\text{Slope of Line AB} = S_{AB} = \frac{y_2 - y_1}{x_2 - x_1} \tag{B.1}$$

$$\text{Center point M} = (a_1, b_1) = \left[\frac{x_1 + x_2}{2}, \frac{y_1 + y_2}{2}\right] \tag{B.2}$$

The equation of the line, L1, which is perpendicular to Line AB at point M can be expressed as:

$$y = S_{L1}(x - a_1) + b_1 \tag{B.3}$$

where

Slope of the Line L1 = $S_{L1} = -\frac{1}{S_{AB}}$

Using the procedure mentioned above, the equation of line L2, which is perpendicular to Line BC at point N can be expressed as:

$$y = S_{L2}(x - a_2) + b_2 \tag{B.4}$$

Where,

$$S_{L2} = -\frac{1}{S_{BC}} = -\frac{x_3 - x_2}{y_3 - y_2}$$

$$a_2 = \frac{x_2 + x_3}{2}\ ,\ \ b_2 = \frac{y_2 + y_3}{2}$$

The lines, L1 and L2 intersect at the center of the curve in figure B.1. The coordinate of the center point, O, can be obtained using equations B.3 and B.4 and expressed as:

$$x_0 = \frac{S_{L1}a_1 - S_{L2}a_2 - b_1 + b_2}{S_{L1} - S_{L2}}$$

$$y_0 = \frac{S_{L1}S_{L2}(a_1 - a_2) - S_{L2}b_1 + S_{L1}b_2}{S_{L1} - S_{L2}} \tag{B.5}$$

The distance from the center point, O, to any of the three points, A, B, and C is the radius of the curve in figure B.1. The radius and the curvature of this curve can be expressed as:

$$R = \sqrt{(x_0 - x_1)^2 + (y_0 - y_1)^2} = \sqrt{(x_0 - x_2)^2 + (y_0 - y_2)^2} = \sqrt{(x_0 - x_3)^2 + (y_0 - y_3)^2}$$

$$K = \frac{1}{R}$$

APPENDIX C

MATLAB PROGRAMS FOR NUMERICAL SOLUTION AND PARAMETRIC STUDY

C1. Closed form Solution to Evaluate Effective Bending and Axial Stiffnesses of Hat Cross-Sections – Matlab Program

```
%%%**inputs**%%%

global angle nply tply r Q11 Q12 Q22 Q66 k theta A1 B1 D1

%%% Laminate 1 - Top Flange Laminate%%%
%%% If laminate is unsymmetric, input laminae in reverse order, %%%
angle = [45 -45 0 0 -45 45]*pi/180;        % Fiber angle - Z-axis rotation
nply = 6;                                  % Number of plies
tply = 0.005;                              % Ply thickness
theta_web = 90*pi/180;                     % Web Angle
b1 = 1;                                    % Width of Top Flange Laminate
H = 1;                                     % Web Height
L = H/sin(theta_web);                      % Length of Web Laminate - Changes with
                                           % Web Angle
b4 = 1;                                    % Width of Bottom Flange Laminate
b5 = b1 + 2*H/tan(theta_web);              % Width of Bottom Laminate
d1 = (H/2) + (nply*tply/2);                % Vertical distance between Mid-plane of
                                           % Top Laminate and Web Mid-height
theta = 0*pi/180;                          % X-rotation for top Laminate is zero

%%% Material Properties- AS4/3501-6 Graphite/Epoxy %%%

E1 = 18.2e6;
E2 = 1.41e6;
G12 = 0.92e6;
v12 = 0.274;
v21 = (E2/E1)*v12;

%%% Calculation of Q-Matrix%%%

Q11 = E1/(1-v12*v21);
Q22 = E2/(1-v12*v21);
Q12 = (E2/(1-v12*v21))*v12;
Q66 = G12;

%%% ABD Matrix (per unit length) at Mid-Plane of Top Laminate %%%

A1 = A;
B1 = B;
D1 = D;
```

```
%%% Multiplying with width of laminate and Axis translation to Mid-height of Web
%%%

A1_bar = b1*A1;
B1_bar = b1*(B1 + d1*A1);
D1_bar = b1*(D1 + 2*d1*B1 + (d1^2)*A1);

%%% Laminate 2 - Left Web Laminate %%%

angle = [45 -45 -45 45]*pi/180;          % Fiber angle - Z-axis rotation
nply = 4;                                % Number of plies
theta = 90*pi/180;                       % X-Axis rotation for Web laminate

%%% ABD Matrix (per unit length) %%%

A2 = A;
B2 = B;
D2 = D;

%%% ABD Matrix at Mid-Height of Web Laminate after integrating along the length
%%%

A2_bar = L*A2;
B2_bar = L*B2;
D2_bar = L*D2 + (1/12)*(L^3)*((sin(theta)).^2)*A2;

%%% Laminate 3 - Right Web Laminate %%%

angle = [45 -45 -45 45]*pi/180;          % Fiber angle - Z-axis rotation
nply = 4;                                % Number of plies
theta = 90*pi/180;                       % X-Axis rotation for Web laminate

%%% ABD Matrix (per unit length) %%%

A3 = A;
B3 = B;
D3 = D;

%%% ABD Matrix at Mid-Height of Web Laminate after integrating along the length
%%%

A3_bar = L*A3;
B3_bar = L*B3;
D3_bar = L*D3 + (1/12)*(L^3)*((sin(theta)).^2)*A3;
```

```
%%% Laminate 4 - Left Bottom Flange Laminate%%%

angle = [45 -45 -45 45 0 0 45 -45 -45 45]*pi/180;   % Fiber angle - Z-axis rotation
nply = 10;                                          % Number of plies
theta = 0*pi/180;                                   % X-Axis rotation for Web laminate
d4 = -((H/2) + (nply*tply/2));                      % Vertical Distance between bottom
                                                    %Flange laminate and Web Mid-height

%%% ABD Matrix (per unit length) at Mid-Plane of Top Laminate %%%

A4 = A;
B4 = B;
D4 = D;

%%% Multiplying with width of laminate and Axis translation to Mid-height of Web
%%%

A4_bar = b4*A4;
B4_bar = b4*(B4 + d4*A4);
D4_bar = b4*(D4 + 2*d4*B4 + (d4^2)*A4);

%%% Laminate 5 - Right Bottom Flange Laminate%%%

angle = [45 -45 -45 45 0 0 45 -45 -45 45]*pi/180;  % Fiber angle - Z-axis rotation
nply = 10;                                         % Number of plies
theta = 0*pi/180;                                  % X-Axis rotation for Web laminate

%%% ABD Matrix (per unit length) at Mid-Plane of Top Laminate %%%

A5 = A;
B5 = B;
D5 = D;

%%% Multiplying with width of laminate and Axis translation to Mid-height of Web
%%%

A5_bar = b4*A5;
B5_bar = b4*(B5 + d4*A5);
D5_bar = b4*(D5 + 2*d4*B5 + (d4^2)*A5);

%%% Laminate 6 - Bottom Laminate%%%

angle = [45 -45 -45 45 0 0]*pi/180;              % Fiber angle - Z-axis rotation
```

```
nply = 6;                                   % Number of plies
theta = 0*pi/180;                           % X-Axis rotation for Web laminate
bot_fl_th_6 = nply*tply;                    % Thickness of Bottom Laminate
d5 = -((H/2) + (nply*tply/2) + (4*0.005));  % Vertical Distance between bottom
laminate and Web Mid-height

%%% ABD Matrix (per unit length) at Mid-Plane of Top Laminate %%%

A6 = A;
B6 = B;
D6 = D;

%%% Multiplying with width of laminate and Axis translation to Mid-height of Web
%%%

A6_bar = b5*A6;
B6_bar = b5*(B6 + d5*A6);
D6_bar = b5*(D6 + 2*d5*B6 + (d5^2)*A6);

%% Summing Stiffnesses about Mid-Height of the Web %%

A_total = A1_bar + A2_bar + A3_bar + A4_bar + A5_bar + A6_bar;

B_total = B1_bar + B2_bar + B3_bar + B4_bar + B5_bar + B6_bar;

D_total = D1_bar + D2_bar + D3_bar + D4_bar + D5_bar + D6_bar;

ABD_total = [A_total B_total;B_total D_total];

abd_total = inv(ABD_total);

%% Axial and Bending Stiffnesses about the Mid-Height of the Web %%

Axial_stiffness_MP = abd_total(4,4)/((abd_total(1,1)*abd_total(4,4)) -
abd_total(1,4)^2)

Bending_stiffness_MP = abd_total(1,1)/((abd_total(1,1)*abd_total(4,4)) -
abd_total(1,4)^2)

%% Location of Centroid and Shear Center from Mid-Plane of the Web %%

Centroid_from_MidPlane = -(abd_total(1,4)/abd_total(4,4));

Shear_Center_from_MidPlane = -(abd_total(3,6)/abd_total(6,6));
```

```
Midplane_from_bottom = bot_fl_th_6 + (4*0.005) + (H/2);

%% Location of Centroid and Shear Center from Middle of Bottom Laminate %%

centroid_from_bottom = Midplane_from_bottom + Centroid_from_MidPlane;

ShearCenter_from_bottom = Midplane_from_bottom + Shear_Center_from_MidPlane;

%% Shifting ABD from Mid-Plane to Neutral Axis %%

A_total_NA = A_total;

B_total_NA = B_total + (-Centroid_from_MidPlane)*A_total;

D_total_NA = D_total + (-2*Centroid_from_MidPlane)*B_total +
((Centroid_from_MidPlane)^2)*A_total;

ABD_total_NA = [A_total_NA B_total_NA;B_total_NA D_total_NA];

abd_total_NA = inv(ABD_total_NA);

%% Axial and Bending Stiffness of the Hat Cross-Section %%

Axial_stiffness_NA = abd_total_NA(4,4)/((abd_total_NA(1,1)*abd_total_NA(4,4)) -
abd_total_NA(1,4)^2)

Bending_stiffness_NA = abd_total_NA(1,1)/((abd_total_NA(1,1)*abd_total_NA(4,4)) -
abd_total_NA(1,4)^2)

%% Unit Force and Moment Resultants obtained from program %%

NT_MT = [128.7447;226.3593;0;-34.5170;-61.2390;0];

e0_k0 = abd_total*NT_MT;

e0 = [e0_k0(1,1);e0_k0(2,1);e0_k0(3,1)];          % Mid-Plane Strains

k0 = [e0_k0(4,1);e0_k0(5,1);e0_k0(6,1)];          % Mid-Plane Curvature
```

C2. Matlab Program to compute Unit Force and Moment Resultants of Equivalent Plate

```
%%%**inputs**%%%

global angle nply tply r Q11 Q12 Q22 Q66 k theta A1 B1 D1

%%% Laminate 1 %%%
%%% If laminate is unsymmetric, input laminae in reverse order, %%%
angle = [45 -45 0 0 -45 45]*pi/180;  %fiber angle
nply = 6;    %number of plies
tply = 0.005; %ply thickness
theta_web = 90*pi/180;
b1 = 1;
H = 1;
L = H/sin(theta_web);
b4 = 1;
b5 = b1 + 2*H/tan(theta_web);
d1 = (H/2) + (nply*tply/2);
theta = 0*pi/180;

T = 100;
MC = 0.01;
Nx = [0;0;0];

%%%Material Properties%%%

E1 = 18.2e6;
E2 = 1.41e6;
G12 = 0.92e6;
v12 = 0.274;
v21 = (E2/E1)*v12;

%%% Calculation of Q-Matrix%%%

Q11 = E1/(1-v12*v21);
Q22 = E2/(1-v12*v21);
Q12 = (E2/(1-v12*v21))*v12;
Q66 = G12;

Q = [Q11 Q12 0;Q12 Q22 0;0 0 Q66];

h = [-0.015 -0.01 -0.005 0 0.005 0.01 0.015];
```

```
QsumNTxx_1 = 0;
QsumNTyy_1 = 0;
QsumNTxy_1 = 0;
QsumMTxx_1 = 0;
QsumMTyy_1 = 0;
QsumMTxy_1 = 0;

for k = 1:nply
QBAR11 = cos(angle(k)).^4*Q11 + sin(angle(k)).^4*cos(theta).^4*Q22 +
2*cos(angle(k)).^2*sin(angle(k)).^2*cos(theta).^2*Q12 +
4*cos(angle(k)).^2*sin(angle(k)).^2*cos(theta).^2*Q66;
QBAR12 = cos(angle(k)).^2*sin(angle(k)).^2*Q11 +
cos(angle(k)).^2*sin(angle(k)).^2*cos(theta).^4*Q22 + (cos(angle(k)).^4 +
sin(angle(k)).^4)*cos(theta).^2*Q12 -
4*cos(angle(k)).^2*sin(angle(k)).^2*cos(theta).^2*Q66;
QBAR16 = cos(angle(k)).^3*sin(angle(k))*Q11 -
cos(angle(k))*sin(angle(k)).^3*cos(theta).^4*Q22 +(cos(angle(k))*sin(angle(k)).^3 -
cos(angle(k)).^3*sin(angle(k)))*cos(theta).^2*Q12 + 2*(cos(angle(k))*sin(angle(k)).^3
- cos(angle(k)).^3*sin(angle(k)))*cos(theta).^2*Q66;
QBAR22 = sin(angle(k)).^4*Q11 + cos(angle(k)).^4*cos(theta).^4*Q22 +
2*cos(angle(k)).^2*sin(angle(k)).^2*cos(theta).^2*Q12 +
4*cos(angle(k)).^2*sin(angle(k)).^2*cos(theta).^2*Q66;
QBAR26 = cos(angle(k))*sin(angle(k)).^3*Q11 -
cos(angle(k)).^3*sin(angle(k))*cos(theta).^4*Q22 + (cos(angle(k)).^3*sin(angle(k)) -
cos(angle(k))*sin(angle(k)).^3)*cos(theta).^2*Q12 + 2*(cos(angle(k)).^3*sin(angle(k))
- cos(angle(k))*sin(angle(k)).^3)*cos(theta).^2*Q66;
QBAR66 = cos(angle(k)).^2*sin(angle(k)).^2*Q11 +
cos(angle(k)).^2*sin(angle(k)).^2*cos(theta).^4*Q22 -
2*cos(angle(k)).^2*sin(angle(k)).^2*cos(theta).^2*Q12 + (cos(angle(k)).^2 -
sin(angle(k)).^2).^2*cos(theta).^2*Q66;

QBAR = [QBAR11 QBAR12 QBAR16;QBAR12 QBAR22 QBAR26;QBAR16
QBAR26 QBAR66];

alpha12 = [-0.5e-6;15e-6;0];

alphaxx = cos(angle(k)).^2*alpha12(1,1) + sin(angle(k)).^2*cos(theta).^2*alpha12(2,1)
- cos(angle(k))*sin(angle(k))*cos(theta)*alpha12(3,1);
alphayy = sin(angle(k)).^2*alpha12(1,1) + cos(angle(k)).^2*cos(theta).^2*alpha12(2,1)
+ cos(angle(k))*sin(angle(k))*cos(theta)*alpha12(3,1);
alphaxy = 2*cos(angle(k))*sin(angle(k))*(alpha12(1,1) - cos(theta).^2*alpha12(2,1)) +
(cos(angle(k)).^2-sin(angle(k)).^2)*cos(theta)*alpha12(3,1);

alphabarxy = [alphaxx;alphayy;alphaxy];
```

```
QsumNTxx_1 = QsumNTxx_1 + ((QBAR11*alphaxx + QBAR12*alphayy +
QBAR16*alphaxy)*(h(k+1)-h(k)));
QsumNTyy_1 = QsumNTyy_1 + ((QBAR12*alphaxx + QBAR22*alphayy +
QBAR26*alphaxy)*(h(k+1)-h(k)));
QsumNTxy_1 = QsumNTxy_1 + ((QBAR16*alphaxx + QBAR26*alphayy +
QBAR66*alphaxy)*(h(k+1)-h(k)));
QsumMTxx_1 = QsumMTxx_1 + 0.5*((QBAR16*alphaxx + QBAR26*alphayy +
QBAR66*alphaxy)*((h(k+1).^2)-(h(k).^2)));
QsumMTyy_1 = QsumMTyy_1 + 0.5*((QBAR12*alphaxx + QBAR22*alphayy +
QBAR26*alphaxy)*((h(k+1).^2)-(h(k).^2)));
QsumMTxy_1 = QsumMTxy_1 + 0.5*((QBAR16*alphaxx + QBAR26*alphayy +
QBAR66*alphaxy)*((h(k+1).^2)-(h(k).^2)));

end

NTxx_mid_1 = T*QsumNTxx_1;
NTyy_mid_1 = T*QsumNTyy_1;
NTxy_mid_1 = T*QsumNTxy_1;

MTxx_mid_1_NTxx_1 = T*QsumNTxx_1*d1;
MTyy_mid_1_NTyy_1 = T*QsumNTyy_1*d1;
MTxy_mid_1_NTxy_1 = T*QsumNTxy_1*d1;

MTxx_mid_1 = T*QsumMTxx_1;
MTyy_mid_1 = T*QsumMTyy_1;
MTxy_mid_1 = T*QsumMTxy_1;

%%% Laminate 2 and 3 %%%

angle = [45 -45 -45 45]*pi/180;  %fiber angle
nply = 4;    %number of plies
theta = 0*pi/180;
h = [-0.01 -0.005 0 0.005 0.01];

QsumNTxx_2 = 0;
QsumNTyy_2 = 0;
QsumNTxy_2 = 0;
QsumMTxx_2 = 0;
QsumMTyy_2 = 0;
QsumMTxy_2 = 0;

for k = 1:nply
```

```
QBAR11 = cos(angle(k)).^4*Q11 + sin(angle(k)).^4*cos(theta).^4*Q22 +
2*cos(angle(k)).^2*sin(angle(k)).^2*cos(theta).^2*Q12 +
4*cos(angle(k)).^2*sin(angle(k)).^2*cos(theta).^2*Q66;
QBAR12 = cos(angle(k)).^2*sin(angle(k)).^2*Q11 +
cos(angle(k)).^2*sin(angle(k)).^2*cos(theta).^4*Q22 + (cos(angle(k)).^4 +
sin(angle(k)).^4)*cos(theta).^2*Q12 -
4*cos(angle(k)).^2*sin(angle(k)).^2*cos(theta).^2*Q66;
QBAR16 = cos(angle(k)).^3*sin(angle(k))*Q11 -
cos(angle(k))*sin(angle(k)).^3*cos(theta).^4*Q22 +(cos(angle(k))*sin(angle(k)).^3 -
cos(angle(k)).^3*sin(angle(k)))*cos(theta).^2*Q12 + 2*(cos(angle(k))*sin(angle(k)).^3
- cos(angle(k)).^3*sin(angle(k)))*cos(theta).^2*Q66;
QBAR22 = sin(angle(k)).^4*Q11 + cos(angle(k)).^4*cos(theta).^4*Q22 +
2*cos(angle(k)).^2*sin(angle(k)).^2*cos(theta).^2*Q12 +
4*cos(angle(k)).^2*sin(angle(k)).^2*cos(theta).^2*Q66;
QBAR26 = cos(angle(k))*sin(angle(k)).^3*Q11 -
cos(angle(k)).^3*sin(angle(k))*cos(theta).^4*Q22 + (cos(angle(k)).^3*sin(angle(k)) -
cos(angle(k))*sin(angle(k)).^3)*cos(theta).^2*Q12 + 2*(cos(angle(k)).^3*sin(angle(k))
- cos(angle(k))*sin(angle(k)).^3)*cos(theta).^2*Q66;
QBAR66 = cos(angle(k)).^2*sin(angle(k)).^2*Q11 +
cos(angle(k)).^2*sin(angle(k)).^2*cos(theta).^4*Q22 -
2*cos(angle(k)).^2*sin(angle(k)).^2*cos(theta).^2*Q12 + (cos(angle(k)).^2 -
sin(angle(k)).^2).^2*cos(theta).^2*Q66;

QBAR = [QBAR11 QBAR12 QBAR16;QBAR12 QBAR22 QBAR26;QBAR16
QBAR26 QBAR66];

alpha12 = [-0.5e-6;15e-6;0];

alphaxx = cos(angle(k)).^2*alpha12(1,1) + sin(angle(k)).^2*cos(theta).^2*alpha12(2,1)
- cos(angle(k))*sin(angle(k))*cos(theta)*alpha12(3,1);
alphayy = sin(angle(k)).^2*alpha12(1,1) + cos(angle(k)).^2*cos(theta).^2*alpha12(2,1)
+ cos(angle(k))*sin(angle(k))*cos(theta)*alpha12(3,1);
alphaxy = 2*cos(angle(k))*sin(angle(k))*(alpha12(1,1) - cos(theta).^2*alpha12(2,1)) +
(cos(angle(k)).^2-sin(angle(k)).^2)*cos(theta)*alpha12(3,1);

alphabarxy = [alphaxx;alphayy;alphaxy];

QsumNTxx_2 = QsumNTxx_2 + ((QBAR11*alphaxx + QBAR12*alphayy +
QBAR16*alphaxy)*(h(k+1)-h(k)));
QsumNTyy_2 = QsumNTyy_2 + ((QBAR12*alphaxx + QBAR22*alphayy +
QBAR26*alphaxy)*(h(k+1)-h(k)));
QsumNTxy_2 = QsumNTxy_2 + ((QBAR16*alphaxx + QBAR26*alphayy +
QBAR66*alphaxy)*(h(k+1)-h(k)));
```

```
QsumMTxx_2 = QsumMTxx_2 + 0.5*((QBAR16*alphaxx + QBAR26*alphayy +
QBAR66*alphaxy)*((h(k+1).^2)-(h(k).^2)));
QsumMTyy_2 = QsumMTyy_2 + 0.5*((QBAR12*alphaxx + QBAR22*alphayy +
QBAR26*alphaxy)*((h(k+1).^2)-(h(k).^2)));
QsumMTxy_2 = QsumMTxy_2 + 0.5*((QBAR16*alphaxx + QBAR26*alphayy +
QBAR66*alphaxy)*((h(k+1).^2)-(h(k).^2)));

end

NTxx_mid_2_3 = 2*T*QsumNTxx_2;
NTyy_mid_2_3 = 2*T*QsumNTyy_2;
NTxy_mid_2_3 = 2*T*QsumNTxy_2;

MTxx_mid_2_3 = 2*T*QsumMTxx_2;
MTyy_mid_2_3 = 2*T*QsumMTyy_2;
MTxy_mid_2_3 = 2*T*QsumMTxy_2;

%%% Laminate 4 and 5%%%

angle = [45 -45 -45 45 0 0 45 -45 -45 45]*pi/180;  %fiber angle
nply = 10;    %number of plies
theta = 0*pi/180;
d4 = -((H/2) + (nply*tply/2))
bot_fl_th_4 = nply*tply;

h = [-0.025 -0.02 -0.015 -0.01 -0.005 0 0.005 0.01 0.015 0.02 0.025];

QsumNTxx_4 = 0;
QsumNTyy_4 = 0;
QsumNTxy_4 = 0;
QsumMTxx_4 = 0;
QsumMTyy_4 = 0;
QsumMTxy_4 = 0;

for k = 1:nply
QBAR11 = cos(angle(k)).^4*Q11 + sin(angle(k)).^4*cos(theta).^4*Q22 +
2*cos(angle(k)).^2*sin(angle(k)).^2*cos(theta).^2*Q12 +
4*cos(angle(k)).^2*sin(angle(k)).^2*cos(theta).^2*Q66;
QBAR12 = cos(angle(k)).^2*sin(angle(k)).^2*Q11 +
cos(angle(k)).^2*sin(angle(k)).^2*cos(theta).^4*Q22 + (cos(angle(k)).^4 +
sin(angle(k)).^4)*cos(theta).^2*Q12 -
4*cos(angle(k)).^2*sin(angle(k)).^2*cos(theta).^2*Q66;
QBAR16 = cos(angle(k)).^3*sin(angle(k))*Q11 -
cos(angle(k))*sin(angle(k)).^3*cos(theta).^4*Q22 +(cos(angle(k))*sin(angle(k)).^3 -
```

```
cos(angle(k)).^3*sin(angle(k)))*cos(theta).^2*Q12 + 2*(cos(angle(k))*sin(angle(k)).^3
- cos(angle(k)).^3*sin(angle(k)))*cos(theta).^2*Q66;
QBAR22 = sin(angle(k)).^4*Q11 + cos(angle(k)).^4*cos(theta).^4*Q22 +
2*cos(angle(k)).^2*sin(angle(k)).^2*cos(theta).^2*Q12 +
4*cos(angle(k)).^2*sin(angle(k)).^2*cos(theta).^2*Q66;
QBAR26 = cos(angle(k))*sin(angle(k)).^3*Q11 -
cos(angle(k)).^3*sin(angle(k))*cos(theta).^4*Q22 + (cos(angle(k)).^3*sin(angle(k)) -
cos(angle(k))*sin(angle(k)).^3)*cos(theta).^2*Q12 + 2*(cos(angle(k)).^3*sin(angle(k))
- cos(angle(k))*sin(angle(k)).^3)*cos(theta).^2*Q66;
QBAR66 = cos(angle(k)).^2*sin(angle(k)).^2*Q11 +
cos(angle(k)).^2*sin(angle(k)).^2*cos(theta).^4*Q22 -
2*cos(angle(k)).^2*sin(angle(k)).^2*cos(theta).^2*Q12 + (cos(angle(k)).^2 -
sin(angle(k)).^2).^2*cos(theta).^2*Q66;

QBAR = [QBAR11 QBAR12 QBAR16;QBAR12 QBAR22 QBAR26;QBAR16
QBAR26 QBAR66];

alpha12 = [-0.5e-6;15e-6;0];

alphaxx = cos(angle(k)).^2*alpha12(1,1) + sin(angle(k)).^2*cos(theta).^2*alpha12(2,1)
- cos(angle(k))*sin(angle(k))*cos(theta)*alpha12(3,1);
alphayy = sin(angle(k)).^2*alpha12(1,1) + cos(angle(k)).^2*cos(theta).^2*alpha12(2,1)
+ cos(angle(k))*sin(angle(k))*cos(theta)*alpha12(3,1);
alphaxy = 2*cos(angle(k))*sin(angle(k))*(alpha12(1,1) - cos(theta).^2*alpha12(2,1)) +
(cos(angle(k)).^2-sin(angle(k)).^2)*cos(theta)*alpha12(3,1);

alphabarxy = [alphaxx;alphayy;alphaxy];

QsumNTxx_4 = QsumNTxx_4 + ((QBAR11*alphaxx + QBAR12*alphayy +
QBAR16*alphaxy)*(h(k+1)-h(k)));
QsumNTyy_4 = QsumNTyy_4 + ((QBAR12*alphaxx + QBAR22*alphayy +
QBAR26*alphaxy)*(h(k+1)-h(k)));
QsumNTxy_4 = QsumNTxy_4 + ((QBAR16*alphaxx + QBAR26*alphayy +
QBAR66*alphaxy)*(h(k+1)-h(k)));
QsumMTxx_4 = QsumMTxx_4 + 0.5*((QBAR16*alphaxx + QBAR26*alphayy +
QBAR66*alphaxy)*((h(k+1).^2)-(h(k).^2)));
QsumMTyy_4 = QsumMTyy_4 + 0.5*((QBAR12*alphaxx + QBAR22*alphayy +
QBAR26*alphaxy)*((h(k+1).^2)-(h(k).^2)));
QsumMTxy_4 = QsumMTxy_4 + 0.5*((QBAR16*alphaxx + QBAR26*alphayy +
QBAR66*alphaxy)*((h(k+1).^2)-(h(k).^2)));

end

NTxx_mid_4_5 = 2*T*QsumNTxx_4;
```

```
NTyy_mid_4_5 = 2*T*QsumNTyy_4;
NTxy_mid_4_5 = 2*T*QsumNTxy_4;

MTxx_mid_4_5_NTxx_4_5 = 2*T*QsumNTxx_4*d4;
MTyy_mid_4_5_NTyy_4_5 = 2*T*QsumNTyy_4*d4;
MTxy_mid_4_5_NTxy_4_5 = 2*T*QsumNTxy_4*d4;

MTxx_mid_4_5 = 2*T*QsumMTxx_4;
MTyy_mid_4_5 = 2*T*QsumMTyy_4;
MTxy_mid_4_5 = 2*T*QsumMTxy_4;

%%% Laminate 6 %%%

angle = [45 -45 -45 45 0 0]*pi/180;  %fiber angle
nply = 6;    %number of plies
theta = 0*pi/180;
bot_fl_th_6 = nply*tply;
d5 = -((H/2) + (nply*tply/2) + bot_fl_th_4)

h = [-0.015 -0.01 -0.005 0 0.005 0.01 0.015];

QsumNTxx_6 = 0;
QsumNTyy_6 = 0;
QsumNTxy_6 = 0;
QsumMTxx_6 = 0;
QsumMTyy_6 = 0;
QsumMTxy_6 = 0;

for k = 1:nply
QBAR11 = cos(angle(k)).^4*Q11 + sin(angle(k)).^4*cos(theta).^4*Q22 +
2*cos(angle(k)).^2*sin(angle(k)).^2*cos(theta).^2*Q12 +
4*cos(angle(k)).^2*sin(angle(k)).^2*cos(theta).^2*Q66;
QBAR12 = cos(angle(k)).^2*sin(angle(k)).^2*Q11 +
cos(angle(k)).^2*sin(angle(k)).^2*cos(theta).^4*Q22 + (cos(angle(k)).^4 +
sin(angle(k)).^4)*cos(theta).^2*Q12 -
4*cos(angle(k)).^2*sin(angle(k)).^2*cos(theta).^2*Q66;
QBAR16 = cos(angle(k)).^3*sin(angle(k))*Q11 -
cos(angle(k))*sin(angle(k)).^3*cos(theta).^4*Q22 +(cos(angle(k))*sin(angle(k)).^3 -
cos(angle(k)).^3*sin(angle(k)))*cos(theta).^2*Q12 + 2*(cos(angle(k))*sin(angle(k)).^3
- cos(angle(k)).^3*sin(angle(k)))*cos(theta).^2*Q66;
QBAR22 = sin(angle(k)).^4*Q11 + cos(angle(k)).^4*cos(theta).^4*Q22 +
2*cos(angle(k)).^2*sin(angle(k)).^2*cos(theta).^2*Q12 +
4*cos(angle(k)).^2*sin(angle(k)).^2*cos(theta).^2*Q66;
```

```
QBAR26 = cos(angle(k))*sin(angle(k)).^3*Q11 -
cos(angle(k)).^3*sin(angle(k))*cos(theta).^4*Q22 + (cos(angle(k)).^3*sin(angle(k)) -
cos(angle(k))*sin(angle(k)).^3)*cos(theta).^2*Q12 + 2*(cos(angle(k)).^3*sin(angle(k))
- cos(angle(k))*sin(angle(k)).^3)*cos(theta).^2*Q66;
QBAR66 = cos(angle(k)).^2*sin(angle(k)).^2*Q11 +
cos(angle(k)).^2*sin(angle(k)).^2*cos(theta).^4*Q22 -
2*cos(angle(k)).^2*sin(angle(k)).^2*cos(theta).^2*Q12 + (cos(angle(k)).^2 -
sin(angle(k)).^2).^2*cos(theta).^2*Q66;

QBAR = [QBAR11 QBAR12 QBAR16;QBAR12 QBAR22 QBAR26;QBAR16
QBAR26 QBAR66];

alpha12 = [-0.5e-6;15e-6;0];

alphaxx = cos(angle(k)).^2*alpha12(1,1) + sin(angle(k)).^2*cos(theta).^2*alpha12(2,1)
- cos(angle(k))*sin(angle(k))*cos(theta)*alpha12(3,1);
alphayy = sin(angle(k)).^2*alpha12(1,1) + cos(angle(k)).^2*cos(theta).^2*alpha12(2,1)
+ cos(angle(k))*sin(angle(k))*cos(theta)*alpha12(3,1);
alphaxy = 2*cos(angle(k))*sin(angle(k))*(alpha12(1,1) - cos(theta).^2*alpha12(2,1)) +
(cos(angle(k)).^2-sin(angle(k)).^2)*cos(theta)*alpha12(3,1);

alphabarxy = [alphaxx;alphayy;alphaxy];

QsumNTxx_6 = QsumNTxx_6 + ((QBAR11*alphaxx + QBAR12*alphayy +
QBAR16*alphaxy)*(h(k+1)-h(k)));
QsumNTyy_6 = QsumNTyy_6 + ((QBAR12*alphaxx + QBAR22*alphayy +
QBAR26*alphaxy)*(h(k+1)-h(k)));
QsumNTxy_6 = QsumNTxy_6 + ((QBAR16*alphaxx + QBAR26*alphayy +
QBAR66*alphaxy)*(h(k+1)-h(k)));
QsumMTxx_6 = QsumMTxx_6 + 0.5*((QBAR16*alphaxx + QBAR26*alphayy +
QBAR66*alphaxy)*((h(k+1).^2)-(h(k).^2)));
QsumMTyy_6= QsumMTyy_6 + 0.5*((QBAR12*alphaxx + QBAR22*alphayy +
QBAR26*alphaxy)*((h(k+1).^2)-(h(k).^2)));
QsumMTxy_6 = QsumMTxy_6 + 0.5*((QBAR16*alphaxx + QBAR26*alphayy +
QBAR66*alphaxy)*((h(k+1).^2)-(h(k).^2)));

end

NTxx_mid_6 = T*QsumNTxx_6;
NTyy_mid_6 = T*QsumNTyy_6;
NTxy_mid_6 = T*QsumNTxy_6;

MTxx_mid_6_NTxx_6 = T*QsumNTxx_6*d5;
MTyy_mid_6_NTyy_6 = T*QsumNTyy_6*d5;
```

```
MTxy_mid_6_NTxy_6 = T*QsumNTxy_6*d5;

MTxx_mid_6 = T*QsumMTxx_6;
MTyy_mid_6 = T*QsumMTyy_6;
MTxy_mid_6 = T*QsumMTxy_6;

NTxx_total = NTxx_mid_1 + NTxx_mid_2_3 + NTxx_mid_4_5 + NTxx_mid_6;
NTyy_total = NTyy_mid_1 + NTyy_mid_2_3 + NTyy_mid_4_5 + NTyy_mid_6;
NTxy_total = NTxy_mid_1 + NTxy_mid_2_3 + NTxy_mid_4_5 + NTxy_mid_6;

MTxx_NTxx = MTxx_mid_1_NTxx_1 + MTxx_mid_4_5_NTxx_4_5 +
MTxx_mid_6_NTxx_6;
MTyy_NTyy = MTyy_mid_1_NTyy_1 + MTyy_mid_4_5_NTyy_4_5 +
MTyy_mid_6_NTyy_6;
MTxy_NTxy = MTxy_mid_1_NTxy_1 + MTxy_mid_4_5_NTxy_4_5 +
MTxy_mid_6_NTxy_6

MTxx_total = MTxx_mid_1 + MTxx_mid_2_3 + MTxx_mid_4_5 + MTxx_mid_6 +
MTxx_NTxx;
MTyy_total = MTyy_mid_1 + MTyy_mid_2_3 + MTyy_mid_4_5 + MTyy_mid_6 +
MTyy_NTyy;
MTxy_total = MTxy_mid_1 + MTxy_mid_2_3 + MTxy_mid_4_5 + MTxy_mid_6 +
MTxy_NTxy;

NT = [NTxx_total;NTyy_total;NTxy_total]
MT = [MTxx_total;MTyy_total;MTxy_total]
```

C3. Matlab Program to Compute Ply Stresses due to Thermal Loading

```
%%%**inputs**%%%
%% web angle = 90 degrees
%%%Material Properties%%%

E1 = 18.2e6;
E2 = 1.41e6;
G12 = 0.92e6;
v12 = 0.274;
v21 = (E2/E1)*v12;
tply = 0.005;

%%% Calculation of Q-Matrix%%%

Q11 = E1/(1-v12*v21);
Q22 = E2/(1-v12*v21);
Q12 = (E2/(1-v12*v21))*v12;
Q66 = G12;

Q = [Q11 Q12 0;Q12 Q22 0;0 0 Q66];

%% angle of ply
angle1 = 45*pi/180;

QBAR11 = cos(angle1).^4*Q11 + sin(angle1).^4*Q22 +
2*cos(angle1).^2*sin(angle1).^2*Q12 + 4*cos(angle1).^2*sin(angle1).^2*Q66;
QBAR12 = (Q11 + Q22 - 4*Q66)*sin(angle1).^2*cos(angle1).^2 +
Q12*(cos(angle1).^4 + sin(angle1).^4);
QBAR16 = (Q11 - Q12 - 2*Q66)*cos(angle1).^3*sin(angle1) - (Q22 - Q12 -
2*Q66)*sin(angle1).^3*cos(angle1);
QBAR22 = sin(angle1).^4*Q11 + cos(angle1).^4*Q22 + 2*(Q12 +
2*Q66)*sin(angle1).^2*cos(angle1).^2;
QBAR26 = (Q11-Q12-2*Q66)*cos(angle1)*sin(angle1).^3 - (Q22-Q12-
2*Q66)*cos(angle1).^3*sin(angle1);
QBAR66 = (Q11+Q22-2*Q12-2*Q66)*sin(angle1).^2*cos(angle1).^2 +
Q66*(sin(angle1).^4 + cos(angle1).^4);

QBAR = [QBAR11 QBAR12 QBAR16;QBAR12 QBAR22 QBAR26;QBAR16
QBAR26 QBAR66];

alpha12 = [-0.5e-6;15e-6;0];

alphaxx = cos(angle1).^2*alpha12(1,1) + sin(angle1).^2*alpha12(2,1);
```

```
alphayy = sin(angle1).^2*alpha12(1,1) + cos(angle1).^2*alpha12(2,1);
alphaxy = 2*cos(angle1)*sin(angle1)*(alpha12(1,1) - alpha12(2,1));

alphabarxy = [alphaxx;alphayy;alphaxy];

T = 100;
zk_top = 0.53;
zk_bottom = zk_top-tply;

%% Mid-plane strain and curvature

e0 = [-0.0379e-3;0.2679e-3;-5.8857e-010];
k0 = [-0.1906e-4;0.3338e-4;-2.1982e-009];

ek_top = e0 + zk_top*k0;

ek_bottom = e0 + zk_bottom*k0;

stressxy_top = QBAR*(ek_top - T*alphabarxy)
stressxy_bottom = QBAR*(ek_bottom - T*alphabarxy)

stress11_top = cos(angle1).^2*stressxy_top(1,1) + sin(angle1).^2*stressxy_top(2,1) +
2*cos(angle1)*sin(angle1)*stressxy_top(3,1);
stress22_top = sin(angle1).^2*stressxy_top(1,1) + cos(angle1).^2*stressxy_top(2,1) -
2*cos(angle1)*sin(angle1)*stressxy_top(3,1);
stress12_top = -cos(angle1)*sin(angle1)*stressxy_top(1,1) +
cos(angle1)*sin(angle1)*stressxy_top(2,1) + (cos(angle1).^2 -
sin(angle1).^2)*stressxy_top(3,1);

stress_12_top = [stress11_top;stress22_top;stress12_top];

stress11_bottom = cos(angle1).^2*stressxy_bottom(1,1) +
sin(angle1).^2*stressxy_bottom(2,1) +
2*cos(angle1)*sin(angle1)*stressxy_bottom(3,1);
stress22_bottom = sin(angle1).^2*stressxy_bottom(1,1) +
cos(angle1).^2*stressxy_bottom(2,1) -
2*cos(angle1)*sin(angle1)*stressxy_bottom(3,1);
stress12_bottom = -cos(angle1)*sin(angle1)*stressxy_bottom(1,1) +
cos(angle1)*sin(angle1)*stressxy_bottom(2,1) + (cos(angle1).^2 -
sin(angle1).^2)*stressxy_bottom(3,1);

stress_12_bottom = [stress11_bottom;stress22_bottom;stress12_bottom];
```

C4. Matlab Program to Compute Ply Stresses due to Applied Moment

```
%%%**inputs**%%%
%% web angle = 45 degrees %%
%%%Material Properties%%%

E1 = 18.2e6;
E2 = 1.41e6;
G12 = 0.92e6;
v12 = 0.274;
v21 = (E2/E1)*v12;
tply = 0.005;

%%% Calculation of Q-Matrix%%%

Q11 = E1/(1-v12*v21);
Q22 = E2/(1-v12*v21);
Q12 = (E2/(1-v12*v21))*v12;
Q66 = G12;

Q = [Q11 Q12 0;Q12 Q22 0;0 0 Q66];

%% angle of ply
angle1 = 45*pi/180;

QBAR11 = cos(angle1).^4*Q11 + sin(angle1).^4*Q22 +
2*cos(angle1).^2*sin(angle1).^2*Q12 + 4*cos(angle1).^2*sin(angle1).^2*Q66;
QBAR12 = (Q11 + Q22 - 4*Q66)*sin(angle1).^2*cos(angle1).^2 +
Q12*(cos(angle1).^4 + sin(angle1).^4);
QBAR16 = (Q11 - Q12 - 2*Q66)*cos(angle1).^3*sin(angle1) - (Q22 - Q12 -
2*Q66)*sin(angle1).^3*cos(angle1);
QBAR22 = sin(angle1).^4*Q11 + cos(angle1).^4*Q22 + 2*(Q12 +
2*Q66)*sin(angle1).^2*cos(angle1).^2;
QBAR26 = (Q11-Q12-2*Q66)*cos(angle1)*sin(angle1).^3 - (Q22-Q12-
2*Q66)*cos(angle1).^3*sin(angle1);
QBAR66 = (Q11+Q22-2*Q12-2*Q66)*sin(angle1).^2*cos(angle1).^2 +
Q66*(sin(angle1).^4 + cos(angle1).^4);

QBAR = [QBAR11 QBAR12 QBAR16;QBAR12 QBAR22 QBAR26;QBAR16
QBAR26 QBAR66];

Mx = 100;
zk_top = 0.53;
```

```
zk_bottom = zk_top-tply;

%% Mid-plane strain and curvature

e0 = [0.1394e-5;-0.1021e-5;0]*Mx;
k0 = [0.4035e-5;-0.2845e-5;0]*Mx;

ek_top = e0 + zk_top*k0;

ek_bottom = e0 + zk_bottom*k0;

%% e = [0.6682e-3;-0.2895e-3;0];

stressxy_top = QBAR*ek_top
stressxy_bottom = QBAR*ek_bottom

%%stress11 = cos(angle1).^2*stressxy(1,1) + sin(angle1).^2*stressxy(2,1) +
2*cos(angle1)*sin(angle1)*stressxy(3,1);
%%stress22 = sin(angle1).^2*stressxy(1,1) + cos(angle1).^2*stressxy(2,1) -
2*cos(angle1)*sin(angle1)*stressxy(3,1);
%%stress12 = -cos(angle1)*sin(angle1)*stressxy(1,1) +
cos(angle1)*sin(angle1)*stressxy(2,1) + (cos(angle1).^2 - sin(angle1).^2)*stressxy(3,1);

stress11_top = cos(angle1).^2*stressxy_top(1,1) + sin(angle1).^2*stressxy_top(2,1) +
2*cos(angle1)*sin(angle1)*stressxy_top(3,1);
stress22_top = sin(angle1).^2*stressxy_top(1,1) + cos(angle1).^2*stressxy_top(2,1) -
2*cos(angle1)*sin(angle1)*stressxy_top(3,1);
stress12_top = -cos(angle1)*sin(angle1)*stressxy_top(1,1) +
cos(angle1)*sin(angle1)*stressxy_top(2,1) + (cos(angle1).^2 -
sin(angle1).^2)*stressxy_top(3,1);

stress_12_top = [stress11_top;stress22_top;stress12_top];

stress11_bottom = cos(angle1).^2*stressxy_bottom(1,1) +
sin(angle1).^2*stressxy_bottom(2,1) +
2*cos(angle1)*sin(angle1)*stressxy_bottom(3,1);
stress22_bottom = sin(angle1).^2*stressxy_bottom(1,1) +
cos(angle1).^2*stressxy_bottom(2,1) -
2*cos(angle1)*sin(angle1)*stressxy_bottom(3,1);
stress12_bottom = -cos(angle1)*sin(angle1)*stressxy_bottom(1,1) +
cos(angle1)*sin(angle1)*stressxy_bottom(2,1) + (cos(angle1).^2 -
sin(angle1).^2)*stressxy_bottom(3,1);

stress_12_bottom = [stress11_bottom;stress22_bottom;stress12_bottom];
```

C5. Functions Used in the Matlab Programs

```
%%%Calculation of [A] stiffness matrix

function Aprime = A()

global angle nply tply r Q11 Q12 Q22 Q66 k theta Aprime A11 A12 A22 A16 A26 A66

A11 = 0;
A12 = 0;
A22 = 0;
A16 = 0;
A26 = 0;
A66 = 0;

for k = 1:nply
      A11 = A11 + (hk(k) - hk(k-1))*(qbar11(k));
end

for k = 1:nply
      A12 = A12 + (hk(k) - hk(k-1))*(qbar12(k));
end

for k = 1:nply
      A22 = A22 + (hk(k) - hk(k-1))*(qbar22(k));
end

for k = 1:nply
      A16 = A16 + (hk(k) - hk(k-1))*(qbar16(k));
end

for k = 1:nply
      A26 = A26 + (hk(k) - hk(k-1))*(qbar26(k));
end

for k = 1:nply
      A66 = A66 + (hk(k) - hk(k-1))*(qbar66(k));
end

Aprime = [A11 A12 A16;A12 A22 A26;A16 A26 A66];
```

```
%%%Calculation of [B] stiffness matrix

function Bprime = B()

global angle nply tply r Q11 Q12 Q22 Q66 k theta Bprime B11 B12 B22 B16 B26 B66

B11 = 0;
B12 = 0;
B22 = 0;
B16 = 0;
B26 = 0;
B66 = 0;

for k = 1:nply
      B11 = B11 + (1/2)*(hk(k)^2 - hk(k-1)^2)*(qbar11(k));
end

for k = 1:nply
      B12 = B12 + (1/2)*(hk(k)^2 - hk(k-1)^2)*(qbar12(k));
end

for k = 1:nply
      B22 = B22 + (1/2)*(hk(k)^2 - hk(k-1)^2)*(qbar22(k));
end

for k = 1:nply
      B16 = B16 + (1/2)*(hk(k)^2 - hk(k-1)^2)*(qbar16(k));
end

for k = 1:nply
      B26 = B26 + (1/2)*(hk(k)^2 - hk(k-1)^2)*(qbar26(k));
end

for k = 1:nply
      B66 = B66 + (1/2)*(hk(k)^2 - hk(k-1)^2)*(qbar66(k));
end

Bprime = [B11 B12 B16;B12 B22 B26;B16 B26 B66];
```

```
%%%Calculation of [D] stiffness matrix

function Dprime = D()

global angle nply tply r Q11 Q12 Q22 Q66 k theta Dprime D11 D12 D22 D16 D26 D66

D11 = 0;
D12 = 0;
D22 = 0;
D16 = 0;
D26 = 0;
D66 = 0;

for k = 1:nply
      D11 = D11 + (1/3)*(hk(k)^3 - hk(k-1)^3)*(qbar11(k));
end

for k = 1:nply
      D12 = D12 + (1/3)*(hk(k)^3 - hk(k-1)^3)*(qbar12(k));
end

for k = 1:nply
      D22 = D22 + (1/3)*(hk(k)^3 - hk(k-1)^3)*(qbar22(k));
end

for k = 1:nply
      D16 = D16 + (1/3)*(hk(k)^3 - hk(k-1)^3)*(qbar16(k));
end

for k = 1:nply
      D26 = D26 + (1/3)*(hk(k)^3 - hk(k-1)^3)*(qbar26(k));
end

for k = 1:nply
      D66 = D66 + (1/3)*(hk(k)^3 - hk(k-1)^3)*(qbar66(k));
end

Dprime = [D11 D12 D16;D12 D22 D26;D16 D26 D66];
```

```
%% Function hk for calculation of layer distance from the center line of the
laminate%%

function y = hk(x)
global nply tply
y = -(nply/2)*tply + x*tply;


%%QBAR Functions%%

function y = QBAR11(x)

global angle Q11 Q12 Q22 Q66 k theta

y = cos(angle(k)).^4*Q11 + sin(angle(k)).^4*cos(theta).^4*Q22 +
2*cos(angle(k)).^2*sin(angle(k)).^2*cos(theta).^2*Q12 +
4*cos(angle(k)).^2*sin(angle(k)).^2*cos(theta).^2*Q66;

function y = QBAR12(x)

global angle Q11 Q12 Q22 Q66 k theta

y = cos(angle(k)).^2*sin(angle(k)).^2*Q11 +
cos(angle(k)).^2*sin(angle(k)).^2*cos(theta).^4*Q22 + (cos(angle(k)).^4 +
sin(angle(k)).^4)*cos(theta).^2*Q12 -
4*cos(angle(k)).^2*sin(angle(k)).^2*cos(theta).^2*Q66;

function y = QBAR16(x)

global angle Q11 Q12 Q22 Q66 k theta

y = cos(angle(k)).^3*sin(angle(k))*Q11 -
cos(angle(k))*sin(angle(k)).^3*cos(theta).^4*Q22 +(cos(angle(k))*sin(angle(k)).^3 -
cos(angle(k)).^3*sin(angle(k)))*cos(theta).^2*Q12 + 2*(cos(angle(k))*sin(angle(k)).^3
- cos(angle(k)).^3*sin(angle(k)))*cos(theta).^2*Q66;

function y = QBAR22(x)

global angle Q11 Q12 Q22 Q66 k theta

y = sin(angle(k)).^4*Q11 + cos(angle(k)).^4*cos(theta).^4*Q22 +
2*cos(angle(k)).^2*sin(angle(k)).^2*cos(theta).^2*Q12 +
4*cos(angle(k)).^2*sin(angle(k)).^2*cos(theta).^2*Q66;
```

```
function y = QBAR26(x)

global angle Q11 Q12 Q22 Q66 k theta

y = cos(angle(k))*sin(angle(k)).^3*Q11 -
cos(angle(k)).^3*sin(angle(k))*cos(theta).^4*Q22 + (cos(angle(k)).^3*sin(angle(k)) -
cos(angle(k))*sin(angle(k)).^3)*cos(theta).^2*Q12 + 2*(cos(angle(k)).^3*sin(angle(k))
- cos(angle(k))*sin(angle(k)).^3)*cos(theta).^2*Q66;

function y = QBAR66(x)

global angle Q11 Q12 Q22 Q66 k theta

y = cos(angle(k)).^2*sin(angle(k)).^2*Q11 +
cos(angle(k)).^2*sin(angle(k)).^2*cos(theta).^4*Q22 -
2*cos(angle(k)).^2*sin(angle(k)).^2*cos(theta).^2*Q12 + (cos(angle(k)).^2 -
sin(angle(k)).^2).^2*cos(theta).^2*Q66;
```

APPENDIX D

FINITE ELEMENT CODE

D1. Ansys Input file to compute Bending Stiffness of Hat Cross-Sections

```
!**** Enables Prompt to Input Variables

*ASK,FLANGBOT, LENGTH OF BOTTOM FLANGE,1
*ASK,WEBH, HEIGHT OF OPEN SECTION,1
*ASK,THETA, ANGLE OF WEB,90
*ASK,FLANGTOP,LENGTH OF TOP FLANGE,1
*ASK,LENGTH, LENGTH OF THE BEAM,20

THETA1 = THETA*3.14159265358979323846264338327795/180

WEBL = WEBH/SIN(THETA1)
WEBW = WEBH/TAN(THETA1)
SECNODE3X = FLANGBOT + WEBW
SECNODE4X = SECNODE3X + FLANGTOP
SECNODE5X = SECNODE4X + WEBW
SECNODE6X = SECNODE5X + FLANGBOT

TPLY = 0.005

E11 = 18.2E6
E22 = 1.41E6
V12 = 0.274
G12 = 0.92E6

/PREP7
ET,1,SHELL91
KEYOPT,1,2,1
KEYOPT,1,5,2
KEYOPT,1,8,1
! DEFINE REAL CONSTANTS HERE
R,1
R,2
R,3
R,4

RMODIF,1,1,6,0
RMODIF,1,13,1,45,TPLY,TPLY,TPLY,TPLY
RMODIF,1,19,1,-45,TPLY,TPLY,TPLY,TPLY
RMODIF,1,25,1,-45,TPLY,TPLY,TPLY,TPLY
RMODIF,1,31,1,45,TPLY,TPLY,TPLY,TPLY
RMODIF,1,37,1,0,TPLY,TPLY,TPLY,TPLY
RMODIF,1,43,1,0,TPLY,TPLY,TPLY,TPLY
```

```
RMODIF,2,1,4,1
RMODIF,2,13,1,45,TPLY,TPLY,TPLY,TPLY
RMODIF,2,19,1,-45,TPLY,TPLY,TPLY,TPLY
RMODIF,2,25,1,-45,TPLY,TPLY,TPLY,TPLY
RMODIF,2,31,1,45,TPLY,TPLY,TPLY,TPLY


RMODIF,3,1,6,1
RMODIF,3,13,1,45,TPLY,TPLY,TPLY,TPLY
RMODIF,3,19,1,-45,TPLY,TPLY,TPLY,TPLY
RMODIF,3,25,1,0,TPLY,TPLY,TPLY,TPLY
RMODIF,3,31,1,0,TPLY,TPLY,TPLY,TPLY
RMODIF,3,37,1,-45,TPLY,TPLY,TPLY,TPLY
RMODIF,3,43,1,45,TPLY,TPLY,TPLY,TPLY

RMODIF,4,1,10,1
RMODIF,4,13,1,45,TPLY,TPLY,TPLY,TPLY
RMODIF,4,19,1,-45,TPLY,TPLY,TPLY,TPLY
RMODIF,4,25,1,-45,TPLY,TPLY,TPLY,TPLY
RMODIF,4,31,1,45,TPLY,TPLY,TPLY,TPLY
RMODIF,4,37,1,0,TPLY,TPLY,TPLY,TPLY
RMODIF,4,43,1,0,TPLY,TPLY,TPLY,TPLY
RMODIF,4,49,1,45,TPLY,TPLY,TPLY,TPLY
RMODIF,4,55,1,-45,TPLY,TPLY,TPLY,TPLY
RMODIF,4,61,1,-45,TPLY,TPLY,TPLY,TPLY
RMODIF,4,67,1,45,TPLY,TPLY,TPLY,TPLY


! DEFINE MATERIAL HERE
UIMP,1,EX,EY,EZ,E11,E22,E22
UIMP,1,PRXY,,,V12,,,
UIMP,1,GXY,,,G12,,,

! *CREATE KEYPOINTS FOR BEAM

K,1,0,0,0
K,2,FLANGBOT,0,0
K,3,SECNODE3X,WEBH,0
K,4,SECNODE4X,WEBH,0
K,5,SECNODE5X,0,0
K,6,SECNODE6X,0,0
K,7,0,0,-LENGTH
K,8,FLANGBOT,0,-LENGTH
```

```
K,9,SECNODE3X,WEBH,-LENGTH
K,10,SECNODE4X,WEBH,-LENGTH
K,11,SECNODE5X,0,-LENGTH
K,12,SECNODE6X,0,-LENGTH

!CREATE AREAS

A,2,5,11,8
A,1,2,8,7
A,5,6,12,11
A,2,3,9,8
A,3,4,10,9
A,5,11,10,4

/VIEW,1,1,1,1
APLOT
!UCS 11 FOR FLANGE
!UCS 12 FOR WEB LEFT
!UCS 13 FOR WEB RIGHT
!UCS 14 FOR NORMAL
/TRAID,RBOT
LOCAL,11,0,,,,0,0,90
LOCAL,12,0,,,,THETA,0,90
LOCAL,13,0,,,,-THETA,0,90
LOCAL,14,0,,,,0,0,0

! NAME FLANGE SECTIONS AND APPLY PROPERTIES
! THIS IS THE LOWER BOTTOM FLANGE
ASEL,S,AREA,,1
AATT,1,1,1,11
! THIS IS THE LOWER LEFT FLANGE
ASEL,S,AREA,,2
AATT,1,4,1,11
! THIS IS THE LOWER RIGHT FLANGE
ASEL,S,AREA,,3
AATT,1,4,1,11
! THIS IS THE LEFT WEB
ASEL,S,AREA,,4
AATT,1,2,1,12
! THIS IS THE RIGHT WEB
ASEL,S,AREA,,6
AATT,1,2,1,13
! THIS IS THE UPPER FLANGE
ASEL,S,AREA,,5
```

```
AATT,1,3,1,11
ALLSEL

! DEFINE SEGMENT PER LINE FOR LONG LINES
LSEL,S,,,2,4,2
LSEL,A,,,7,9,2
LSEL,A,,,12,15,3
CM,LONGLINE,LINE
LESIZE,ALL,,,30,,1
! DEFINE SEGMENT PER LINE FOR WEB LINES
LSEL,S,,,11,13,2
LSEL,A,,,17,18,1
CM,WEBLINE,LINE
LESIZE,ALL,,,6,,1

! DEFINE SEGMENT PER LINE FOR FLANGE LINES
ALLSEL
CMSEL,U,LONGLINE
CMSEL,U,WEBLINE
LESIZE,ALL,,,8,,1
ALLSEL
/VIEW,1,1,1,1
/ANG,1
! MESH HERE
AMESH,ALL
EPLOT
ESYS,14

!APPLY FORCE

!FORM RIGID SECTIONS AT THE ENDS
NSEL,,LOC,Z,0
CERIG,2830,ALL,ALL
F,2830,FZ,100
F,10,FZ,-100
ALLSEL

! BFUNIF,TEMP,100

!FORM RIGID SECTIONS AT THE ENDS
NSEL,,LOC,Z,0
D,ALL, , , , , ,UX,, , , ,
ALLSEL
```

```
NSEL,,LOC,Z,-LENGTH
D,ALL,ALL
ALLSEL

/SOLU
SOLVE
FINISH

!AVPRIN,0,0,

!PLNSOL,S,Z,2,1

NSEL,S,LOC,Z,-10
NSEL,A,LOC,Z,(-10-(2/3))
NSEL,A,LOC,Z,(-10-(4/3))
ESLN

!ESEL,R,REAL,,1,4,1
!ESEL,U,REAL,,3
/REPLOT
```

REFERENCES

[1]. GangaRao, H., Thippeswamy, H., Shekar, V. and Craigo, C., 1999, Development of Glass Fiber Reinforced Polymer Composite Bridge Deck, *SAMPE Journal*, V 35, n 4.

[2]. Skudra, A. M., A. A. Kruklinsh, F. Y. Bulavs, and M. R. Gurvich, 1991, *Structural Analysis of Composite Beam Systems*, Technomic, Lancaster, PA.

[3]. Vasiliev, V. V. and R. M. Jones, 1993, Chapter 4 in *Mechanics of Composite Structures*, Taylor & Francis, Washinton, DC.

[4} Barbero, E.J., 1998, chapter 8 in *Introduction to Composite Materials Design*, Taylor & Francis, Washinton, DC.

[5]. Kollar, L. P. and G. S. Springer, 2003, Chapter 6 & 7 in *Mechanics of Composite Structures* , Cambridge University Press, UK.

[6]. Hodges, D. H., 2006 *Nonlinear Composite Beam Theory*, AIAA, Washington, D.C.

[7]. McGhee, K.K., Barton, F.W and Mckeel, W.T., 1991, "Optimum Design of Composite Bridge Deck Panels," Advanced Composite Materials in Civil Engineering Structures, Proceedings of the Specialty Conference, A.S.C.E., Las Vegas, Nevada,

[8]. Henry, J.A., 1985, *Deck Girders System for Highway Bridges Using Fiber Reinforced Plastics*, Master's Thesis, North Carolina State University, NC.

[9]. Ahmad, S.H. and J. M. Plecnik, 1989, "Transfer of Composite Technology to Design and Construction of Bridges," *U.S. DOT Report*, September.

[10]. Zureick, A., 1997, "Fiber-Reinforced Polymeric Bridge Decks," Proceedings of the National seminar on Advanced Composite Material Bridges, FHWA, 1997.

[11]. Chan, W.S. and K.C. Demirhan, 2000, "A Simple Closed-Form Solution of Bending Stiffness for Laminated Composite Tubes", J. of Reinforced Plastic & Composites, Vol. 19, Nl. 4, pp. 278-291.

[12]. Lin, C. Y. and W.S. Chan, 2002, "A Simple Analytical Method for Analyzing Laminated Composites Elliptical Tubes", Proceedings of the 17th Technical Conference of American Society of Composites.

[13]. Swanson, S. R. 1997, Chapter 7 in *Introduction to Design and Analysis with Advanced Composite Materials* , Prentice Hall, New Jersey.

[14]. Hussein, R., Fazio, P. and Ha, K. (1992), "Effects of Bonding Stiffness on Thermal Stresses in Sandwich Panels.", Journal of Aerospace Engineering, Vol. 5, No. 4, October 1992.

[15]. Krit Laosiriphong., 2004, Theoretical and Experimental Analysis of FRP Bridge Decks under Thermal Loads, Doctoral Dissertation, West Virginia University, WV.

[16] Isaac, M. Daniel and Ori, Ishai., "Engineering Mechanics of Composite Materials", Oxford University Press, Inc.,1994.

[17]. Swanson, S. R. 1997, Chapter 6 and 7 in *Introduction to Design and Analysis with Advanced Composite Materials* , Prentice Hall, New Jersey.

[18]. Chan, W. S. and Chou, C. J., 1995, "Effects of Delamination and Ply Fiber Waviness on Effective Axial and Bending Stiffness in Composite Laminates", Composite Structures, 30, Pp 299-306.

[19]. ANSYS10.0 User Manual

[20]. Drummond, A. Jeffrey., 1995, "Fabrication, analysis, and experimentation of a practically constructed laminated composite I-beam under pure bending", J. of Thermoplastic Composite Materials, Vol. 12/May 1999, Pp 177-189.

BIOGRAPHICAL INFORMATION

Kashif Ali Nayyer Syed was born on January 6, 1979 in Hyderabad, India. He received his B.S. degree in Civil Engineering from Osmania University, Hyderabad, India in May, 2000. He joined The University of Texas at Arlington in August 2000 for Master's program with Graduate Teaching Assistantship and graduated in 2002.

He received Hermann's Scholarship for four years to pursue for the doctoral degree along with teaching and research assistantship. He also participated in internships to acquire industrial experience. He received his doctorate in Civil Engineering from the University of Texas at Arlington in December 2006.

His research interests include composite material analysis and design, finite element analysis, fracture mechanics, structural dynamics, structural analysis and design and computer aided engineering.